

A revised Gaussian pencil beam model for calculation of the in-water dose caused by clinical electron-beam irradiation

Akira Iwasaki, Shingo Terashima, Shigenobu Kimura, Kohji Sutoh, Kazuo Kamimura, Yoichiro Hosokawa, Masanori Miyazawa , and Tatsuo Tabata

<http://dx.doi.org/10.14312/2399-8172.2022-1>

Appendix A

Comments on the σ_r and σ_z^p functions

For a pencil beam irradiation to a water phantom, we take X and Y rectangular coordinate axes on a plane at a phantom depth Z along the beam axis, where the X and Y origins are taken at the same point on the beam axis. For pencil beam algorithms based on the multiple scattering theory, the two sigma functions of $\sigma_r^2(Z)$ and $\sigma^2(Z)$ are introduced, where $\sigma_r^2(Z)$ is the mean square radial displacement of electrons as a result of multiple Coulomb scattering on the Z -plane, and $\sigma^2(Z)$ is the mean square lateral displacement ($\overline{\Delta x^2}$ or $\overline{\Delta y^2}$) projected on to the X -axis or on to the Y -axis, respectively, at depth Z [1, 8]. Letting $\overline{\Delta r^2} = \overline{\Delta x^2} + \overline{\Delta y^2}$ and $\overline{\Delta x^2} = \overline{\Delta y^2}$, we obtain $\sigma_r^2(Z) = 2\sigma_x^2(Z) = 2\sigma_y^2(Z) [= 2\sigma^2(Z)]$. Accordingly, equation (10) can be rewritten as

$$\begin{aligned} \Delta D(X_c, Y_c, Z_c) &= D_{\text{para}}(0, 0, Z_c^{\text{fan}} : A_c = \infty) \\ &\times \frac{1}{4} \left(\operatorname{erf} \frac{\frac{\Delta X'_c}{2} + (X_c - X'_c)}{\sqrt{2}\sigma(Z_c^{\text{fan}})} + \operatorname{erf} \frac{\frac{\Delta X'_c}{2} - (X_c - X'_c)}{\sqrt{2}\sigma(Z_c^{\text{fan}})} \right) \\ &\left(\operatorname{erf} \frac{\frac{\Delta Y'_c}{2} + (Y_c - Y'_c)}{\sqrt{2}\sigma(Z_c^{\text{fan}})} + \operatorname{erf} \frac{\frac{\Delta Y'_c}{2} - (Y_c - Y'_c)}{\sqrt{2}\sigma(Z_c^{\text{fan}})} \right) \end{aligned} \quad (\text{Eq. A1})$$

By examining Appendix 3 (Determination of treatment beam parameter σ_z^p) in the paper by Bruinvis et al. [7], we can tell the equality of $\sigma_r(Z) = \sigma_z^p$.

A revised Gaussian pencil beam model for calculation of the in-water dose caused by clinical electron-beam irradiation

Akira Iwasaki, Shingo Terashima, Shigenobu Kimura, Kohji Sutoh, Kazuo Kamimura, Yoichiro Hosokawa, Masanori Miyazawa , and Tatsuo Tabata

<http://dx.doi.org/10.14312/2399-8172.2022-1>

Supplementary Table 1 Values of the factors used to rebuild the DD and OAD datasets caused by the direct-plus-indirect electron beams. The DD datasets were obtained from figs. 3(a), 5(a), and 3(d) in the W-K eMC dose work in Ref. (5); and the OAD datasets were similarly obtained from figs. 3(b), 3(c), 5(b), 5(c), 3(e), and 3(f), where the stepped and the dotted DD and OAD curves were yielded, respectively, using (i) the standard eMC simulation and (ii) the commercial TPS. It should be noted that the values of $R_p^{MC}(E)$ to $c_2(E)$ are mainly derived from the DD datasets and only the values of $R_{scale}^{OAD}(Z_c)$ are derived from the OAD datasets.

<i>W-K eMC DD & OAD datasets</i>	<i>E</i>	<i>A_{appl}</i>	<i>SSD_{eff}</i>	<i>R_p^{ICRU}(E)</i>	<i>R_p^{MC}(E)</i>	<i>FAC_{adjust}(E)</i>	<i>Z₁(E)</i>	<i>Z₂(E)</i>	<i>θ₀(E)</i>	<i>W_a(E)</i>
<i>for the direct-plus-indirect electron beams (KK=13-24)</i>	<i>(MeV)</i>	<i>(cm²)</i>	<i>(cm)</i>	<i>(cm)</i>	<i>(cm)</i>	<i>(no unit)</i>	<i>(cm)</i>	<i>(cm)</i>	<i>(rad)</i>	<i>(no unit)</i>
<i>(i) Using the standard eMC (in stepped curves)</i>										
KK=13: fig. 3(b)-OAD ($Z_c=1$ cm) under fig. 3(a)-DD	6	10 × 10	82.9	2.834	3.364	0.894	1.7	2.5	1.76	0.0942
KK=14: fig. 3(c)-OAD ($Z_c=5$ cm) under fig. 3(a)-DD	6	10 × 10	82.9	2.834	3.364	0.894	1.7	2.5	1.76	0.0942
KK=15 fig. 5(b)-OAD ($Z_c=2$ cm) under fig. 5(a)-DD	12	10 × 10/14 × 14	91.5	5.915	6.018	0.878	1.5	4.5	1.56	0.117

KK=16: fig. 5(c)-OAD ($Z_c=10$ cm) under fig. 5(a)-DD	12	$10 \times 10/14 \times 14$	91.5	5.915	6.018	0.878	1.5	4.5	1.56	0.117
KK=17: fig. 3(e)-OAD ($Z_c=3$ cm) under fig. 3(d)-DD	18	10×10	86.9	8.996	8.506	0.779	0.9	9.0	1.55	0.233
KK=18: fig. 3(f)-OAD ($Z_c=15$ cm) under fig. 3(d)-DD	18	10×10	86.9	8.996	8.506	0.779	0.9	9.0	1.55	0.233
<i>(ii) Using the commercial eMC (in Dotted Curves)</i>										
KK=19: fig. 3(b)-OAD ($Z_c=1$ cm) under fig. 3(a)-DD	6	10×10	82.9	2.834	3.364	0.909	1.7	2.5	1.764	0.0716
KK=20: fig. 3(c)-OAD ($Z_c=5$ cm) under fig. 3(a)-DD	6	10×10	82.9	2.834	3.364	0.909	1.7	2.5	1.764	0.0716
KK=21: fig. 5(b)-OAD ($Z_c=2$ cm) under fig. 5(a)-DD	12	$10 \times 10/14 \times 14$	91.5	5.915	6.000	0.887	1.75	4.5	1.62	0.103
KK=22: fig. 5(c)-OAD ($Z_c=10$ cm) under fig. 5(a)-DD	12	$10 \times 10/14 \times 14$	91.5	5.915	6.000	0.887	1.75	4.5	1.62	0.103
KK=23: fig. 3(e)-OAD ($Z_c=3$ cm) under fig. 3(d)-DD	18	10×10	86.9	8.996	8.530	0.795	0.9	9.0	0.163	0.209
KK=24: fig. 3(f)-OAD ($Z_c=15$ cm) under fig. 3(d)-DD	18	10×10	86.9	8.996	8.530	0.795	0.9	9.0	0.163	0.209
<i>W-K eMC DD & OAD datasets</i>		$S_c^{eff}(Z_c, E)$	$a_1(E)$	$b_1(E)$	$c_1(E)$	$T_0(Z_c, E)$	$a_2(E)$	$b_2(E)$	$c_2(E)$	$R_{scale}^{OAD}(Z_c)$
<i>for the direct-plus-indirect electron beams (KK=13-24)</i>		(cm)	(cm)	(no unit)	(no unit)	(cm)	(cm)	(no unit)	(no unit)	(no unit)
<i>(i) Using the standard eMC (in stepped curves)</i>										
KK=13: fig. 3(b)-OAD ($Z_c=1$ cm) under fig. 3(a)-DD	13.40	3.72E-07	17.40	9.86E-03	3.00	6.17E-31	70.66	6.60E-03	0.988	

KK=14: fig. 3(c)-OAD ($Z_c=5$ cm) under fig. 3(a)-DD	17.70	3.72E-07	17.40	9.86E-03	6.38	6.17E-31	70.66	6.60E-03	0.159
KK=15 fig. 5(b)-OAD ($Z_c=2$ cm) under fig. 5(a)-DD	12.41	1.52E-22	52.45	8.56E-03	2.10	1.28E-37	84.86	1.40E-02	0.979
KK=16: fig. 5(c)-OAD ($Z_c=10$ cm) under fig. 5(a)-DD	25.80	1.52E-22	52.45	8.56E-03	14.8	1.28E-37	84.86	1.40E-02	0.214
KK=17: fig. 3(e)-OAD ($Z_c=3$ cm) under fig. 3(d)-DD	13.20	3.17E-23	53.88	8.50E-03	2.56	9.02E-37	82.75	1.30E-02	0.997
KK=18: fig. 3(f)-OAD ($Z_c=15$ cm) under fig. 3(d)-DD	27.92	3.17E-23	53.88	8.50E-03	15.10	9.02E-37	82.75	1.30E-02	1.21E+02
<i>(ii) Using the commercial eMC (in dotted curves)</i>									
KK=19: fig. 3(b)-OAD ($Z_c=1$ cm) under fig. 3(a)-DD	13.36	2.02E-07	18.01	9.88E-03	2.81	3.69E-38	87.23	6.01E-03	0.991
KK=20: fig. 3(c)-OAD ($Z_c =5$ cm) under fig. 3(a)-DD	17.83	2.02E-07	18.01	9.88E-03	6.56	3.69E-38	87.23	6.01E-03	0.156
KK=21: fig. 5(b)-OAD ($Z_c=2$ cm) under fig. 5(a)-DD	12.43	3.28E-16	37.95	8.37E-03	2.10	7.01E-35	78.78	1.10E-02	0.979
KK=22: fig. 5(c)-OAD ($Z_c=10$ cm) under fig. 5(a)-DD	20.86	3.28E-16	37.95	8.37E-03	8.67	7.01E-35	78.78	1.10E-02	0.180
KK=23: fig. 3(e)-OAD ($Z_c=3$ cm) under fig. 3(d)-DD	13.20	7.13E-24	55.36	8.50E-03	2.50	2.87E-37	83.85	1.30E-02	0.999
KK=24: fig. 3(f)-OAD ($Z_c=15$ cm) under fig. 3(d)-DD	28.50	7.13E-24	55.36	8.50E-03	15.10	2.87E-37	83.85	1.30E-02	1.72E+02

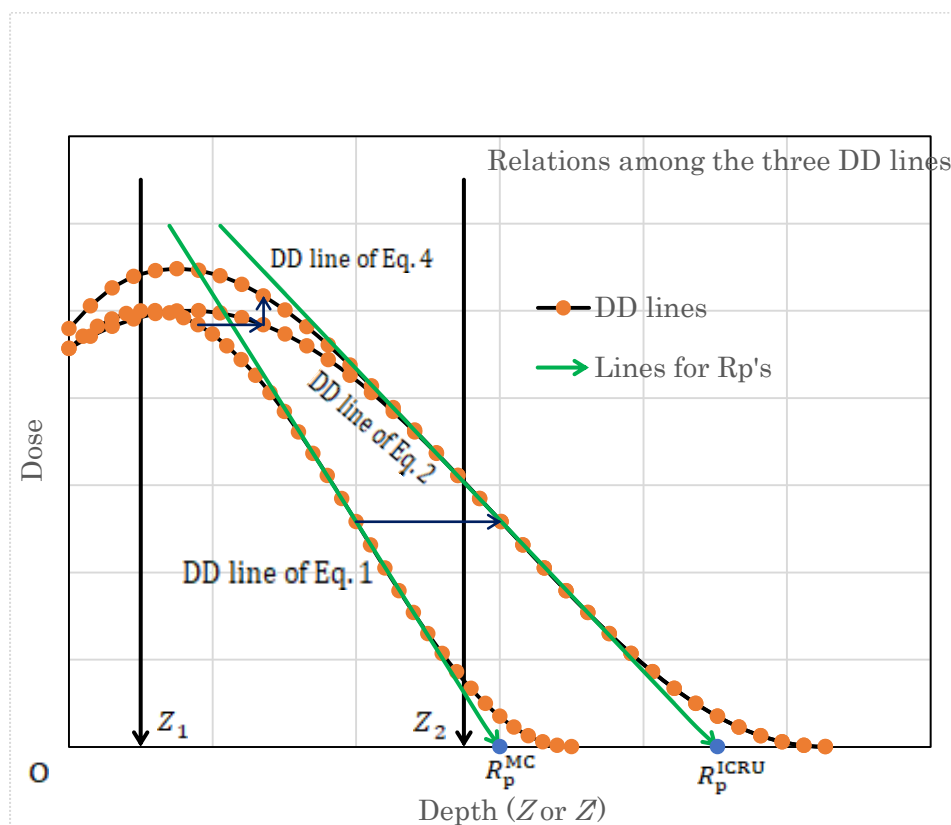
Supplementary 2 Values of dimensionless parameters $a(E)$, $b(E)$, $c(E)$, $d(E)$, and $e(E)$ in Eq. 13 for $E = 6, 10, 14$, and 20 MeV.

	$E = 6 \text{ MeV}$	$E = 10 \text{ MeV}$	$E = 14 \text{ MeV}$	$E = 20 \text{ MeV}$
$a(E)$	5.050×10^{-2}	3.283×10^{-2}	1.940×10^{-2}	1.411×10^{-2}
$b(E)$	0.270	0.252	0.203	0.174
$c(E)$	1.562	1.996	1.836	1.760
$d(E)$	1.051	0.839	0.951	0.985
$e(E)$	3.256	2.804	3.748	2.373

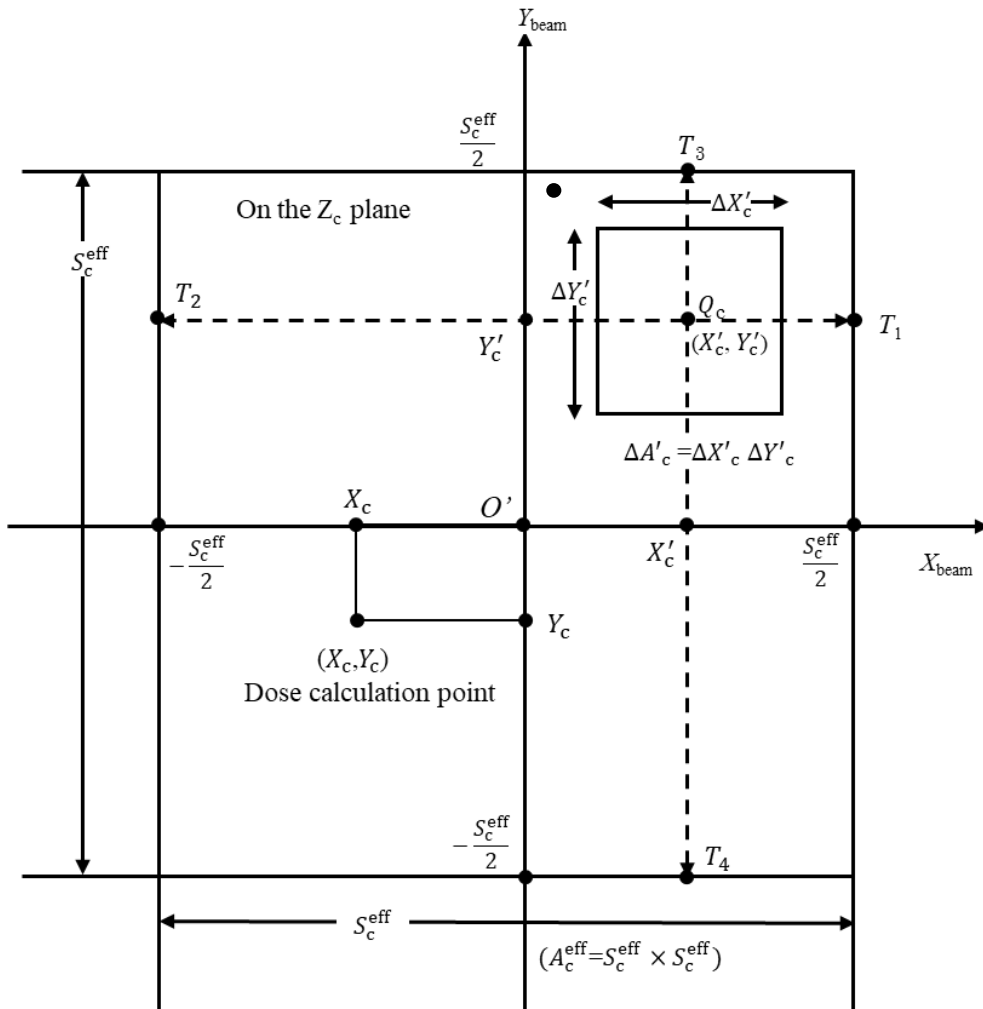
A revised Gaussian pencil beam model for calculation of the in-water dose caused by clinical electron-beam irradiation

Akira Iwasaki, Shingo Terashima, Shigenobu Kimura, Kohji Sutoh, Kazuo Kamimura, Yoichiro Hosokawa, Masanori Miyazawa, and Tatsuo Tabata

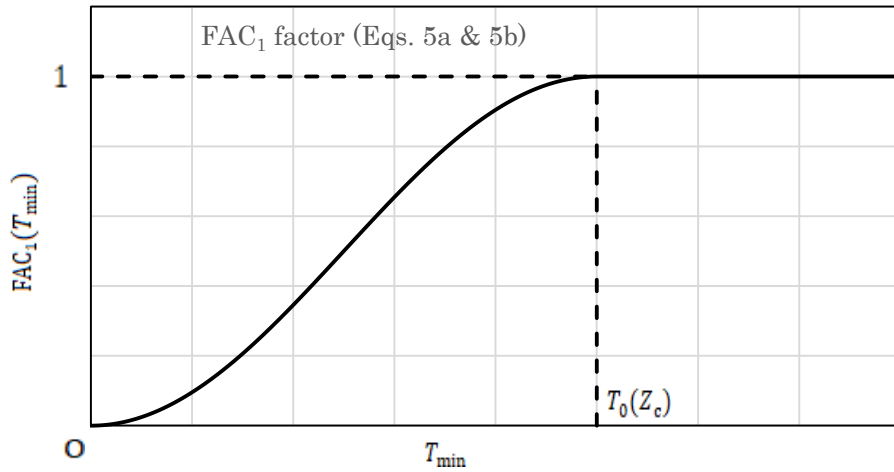
<http://dx.doi.org/10.14312/2399-8172.2022-1>



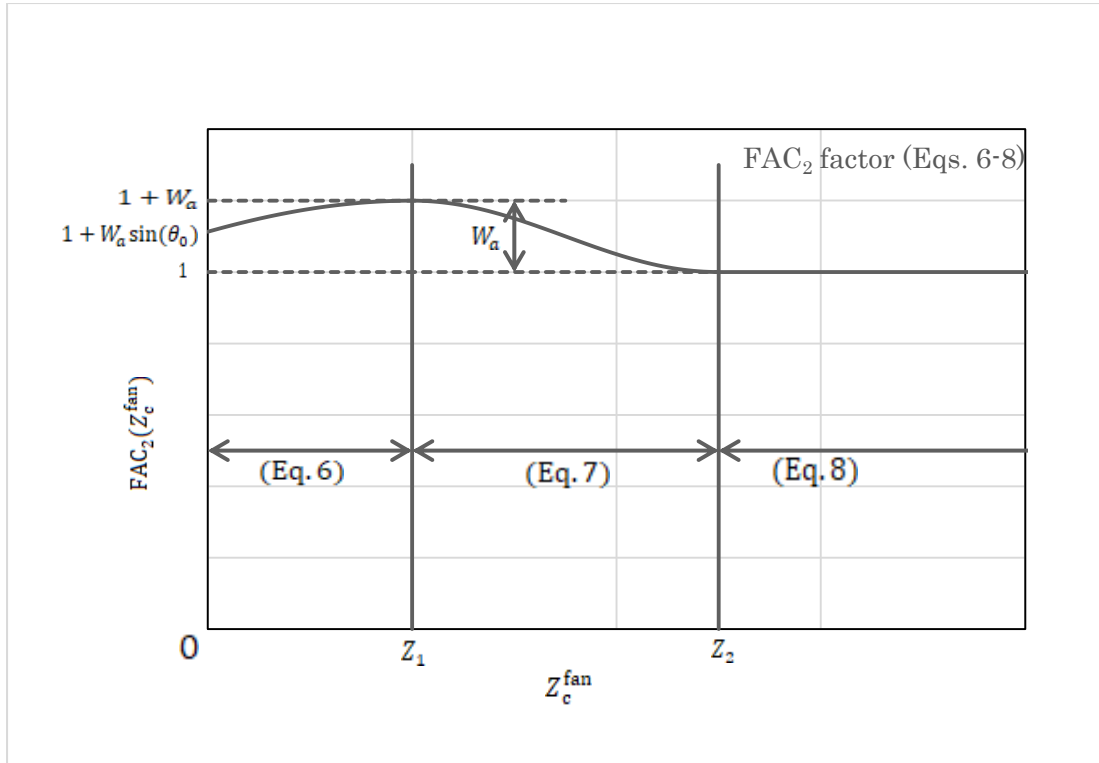
Supplementary Figure 1 Diagram showing how to obtain the final depth-dose curve $D_{\text{para}}(0,0,Z: A_0 = \infty)$ of Eq. 4 via the depth-dose curve of $D'_{\text{para}}(0,0,Z: A_0 = \infty)$ of Eq. 2 that is yielded from the depth-dose curve $D'_{\text{para}}(0,0,Z': A_0)$ of Eq. 1 using the relation of $Z = Z' \times (R_p^{\text{ICRU}} / R_p^{\text{MC}})$. It should also be noted that the final depth-dose curve $D_{\text{para}}(0,0,Z: A_0 = \infty)$ is yielded by modifying the depth-dose curve of $D'_{\text{para}}(0,0,Z: A_0 = \infty)$ in Eq. 4 by using the three factors of $\text{FAC}_{\text{adjust}}$ (Supplementary Tables 1 and 2), FAC_1 (Eqs. 5a & 5b), and FAC_2 (Eqs. 6-8).



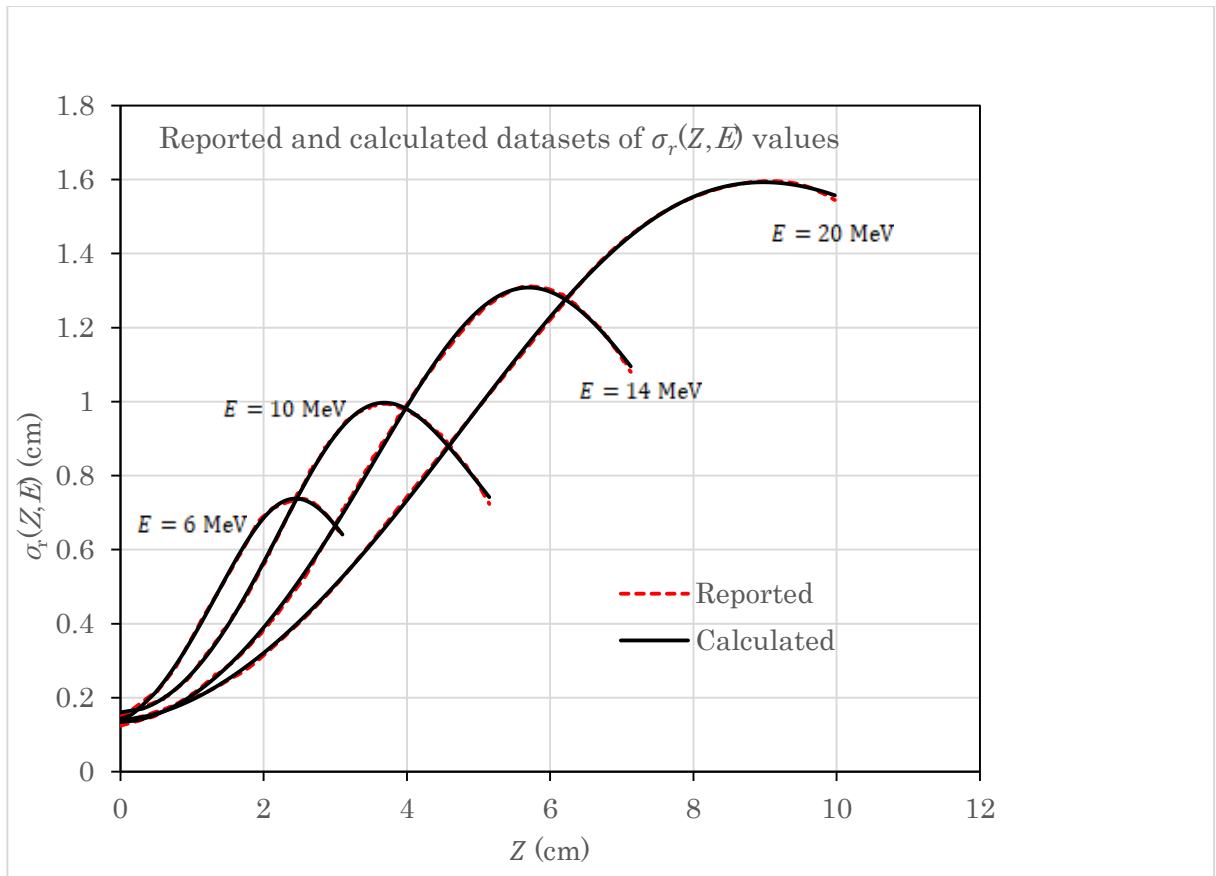
Supplementary Figure 2 Diagram showing how the geometric symbols are used for calculation of the $\text{FAC}_1(T_{\min}; Z_c, A_c^{\text{eff}})$ factor for point (X'_c, Y'_c) , where the whole of $\Delta A'_c = \Delta X'_c \Delta Y'_c$ is set inside the field of $A_c^{\text{eff}} = S_c^{\text{eff}} \times S_c^{\text{eff}}$ on the Z_c plane. It should be noted that T_{\min} expresses the minimum among the values of (T_1, T_2, T_3, T_4) , expressing the distances to each of the four square sides of A_c^{eff} from point (X'_c, Y'_c) . The dose calculation point (X_c, Y_c) may be set at any position on the Z_c plane.



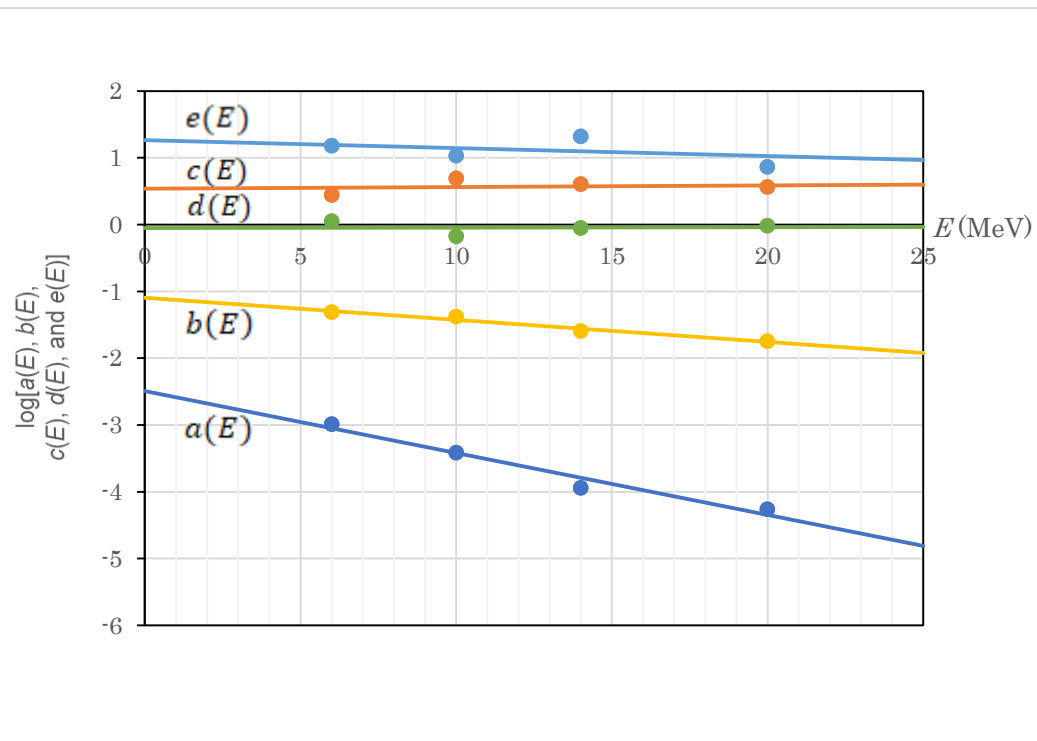
Supplementary Figure 3 Diagram showing how $\text{FAC}_1(T_{\min}; Z_c, A_c^{\text{eff}})$ varies with T_{\min} for a given value of $T_0(Z_c; A_c^{\text{eff}})$.



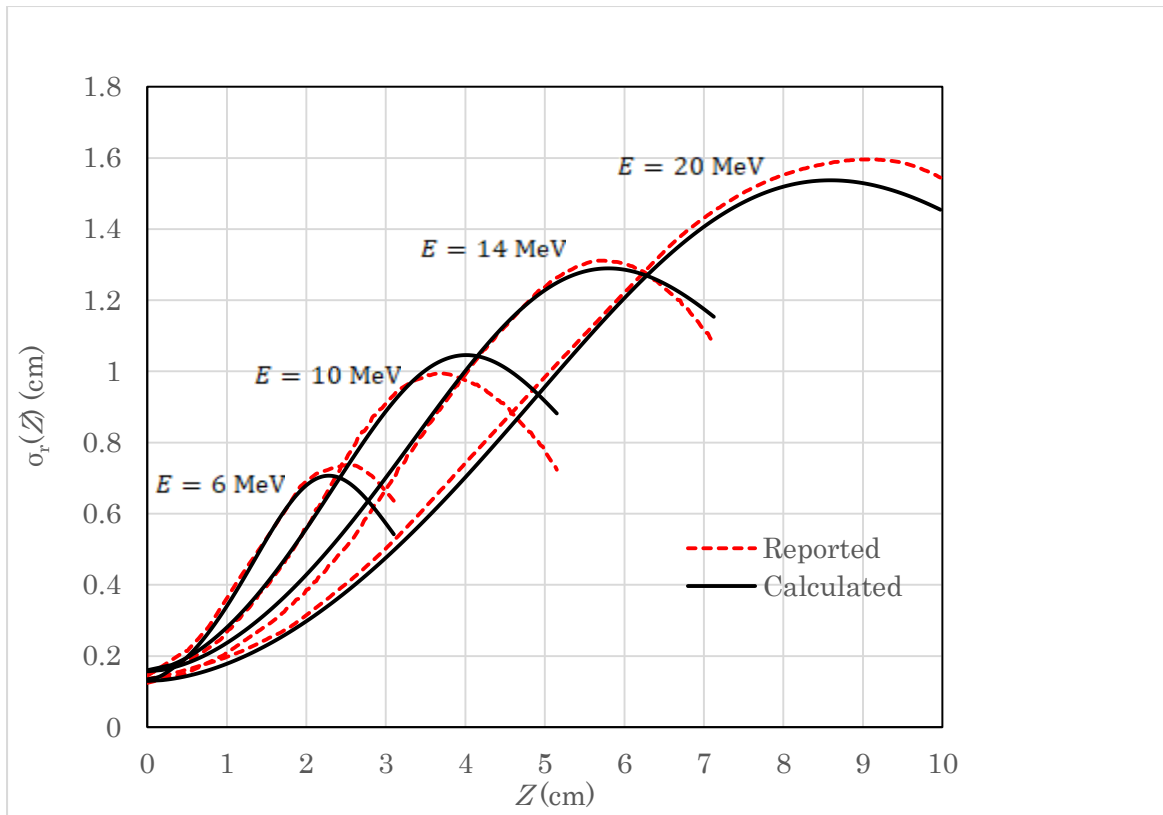
Supplementary Figure 4 Diagram showing how $\text{FAC}_2(Z_c^{\text{fan}}; Z_c, A_c^{\text{eff}})$ varies with Z_c^{fan} using Eqs. 6-8.



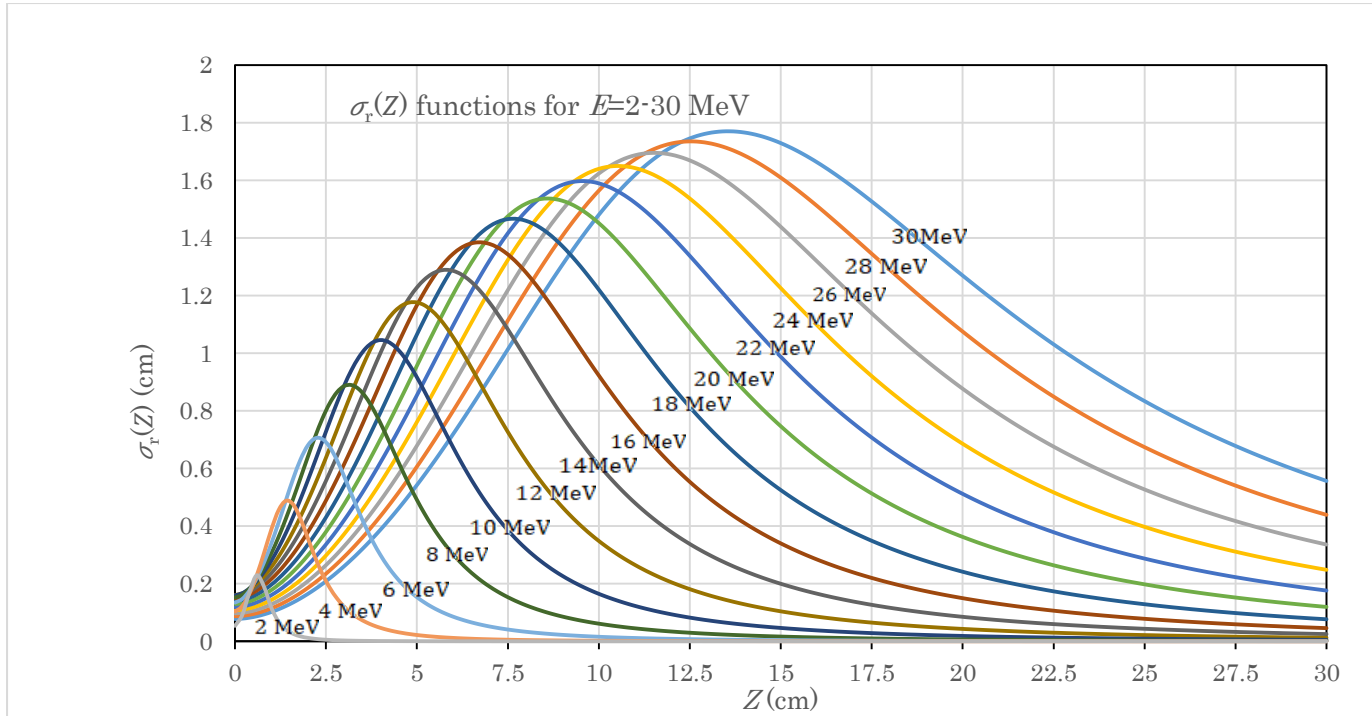
Supplementary Figure 5 Dependence of the $\sigma_r(Z, E)$ function on depth (Z) for each of $E=6, 10, 14$, and 20 MeV electron beams. Solid curves show Eq. 13 with the corresponding sets of $a(E)$ - $e(E)$ values in Supplementary Table 2. Broken curves are the data reported by Bruinvis *et al.*



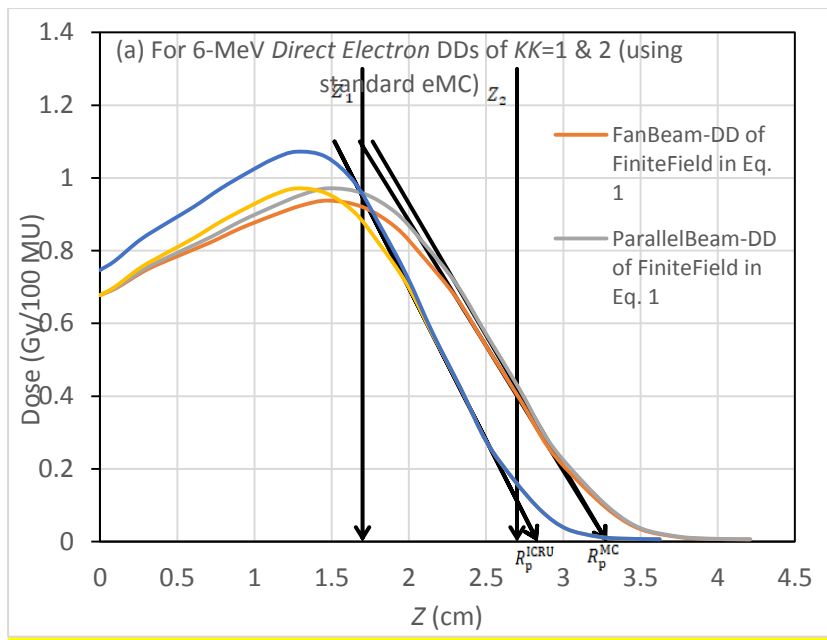
Supplementary Figure 6 Dependence of the $\log[a(E)]$, $\log[b(E)]$, $\log[c(E)]$, $\log[d(E)]$, and $\log[e(E)]$ functions on E . Straight lines show Eqs. 15-19; and dots, the corresponding datasets of $a(E)$ - $e(E)$ in Table 2. Relatively large differences between the equation and dataset arise for the $e(E)$ function.



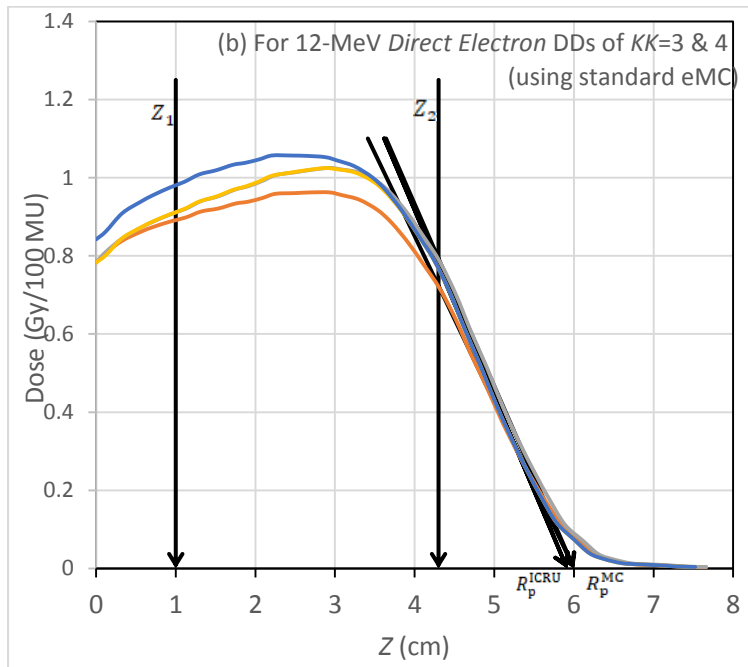
Supplementary Figure 7 Dependence of the $\sigma_r(Z)$ functions on depth (Z) for $E=6, 10, 14$, and 20 MeV. The solid curves show the generalized formula, Eq. 13 with Eqs. 15-19. The broken curves are the data reported by Bruinvis et al.



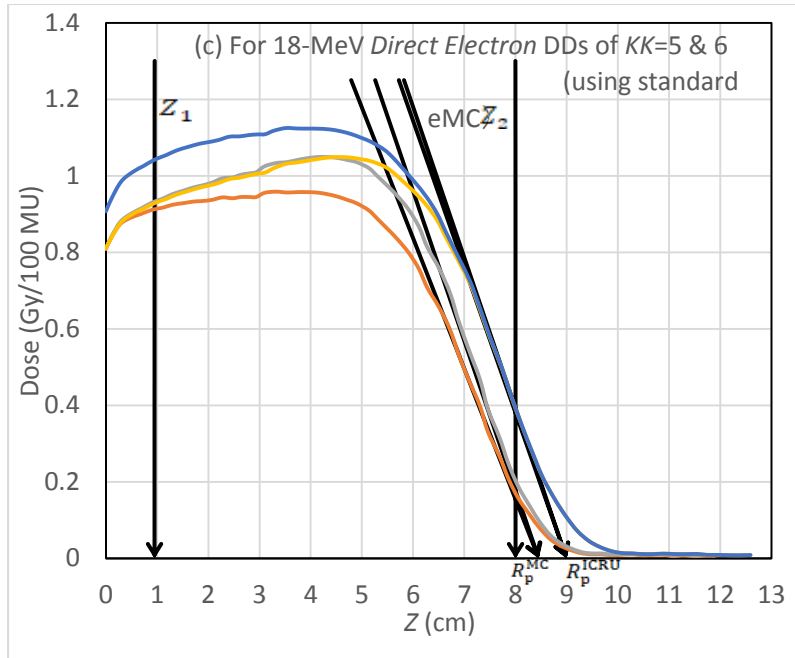
Supplementary Figure 8 Diagram showing the curves of $\sigma_r(Z)$ generated using Eq. 13 with the $a(E)$ - $e(E)$ functions of Eqs. 15-19 for $E = 2\text{-}30 \text{ MeV}$ at intervals of 2 MeV.



(a)

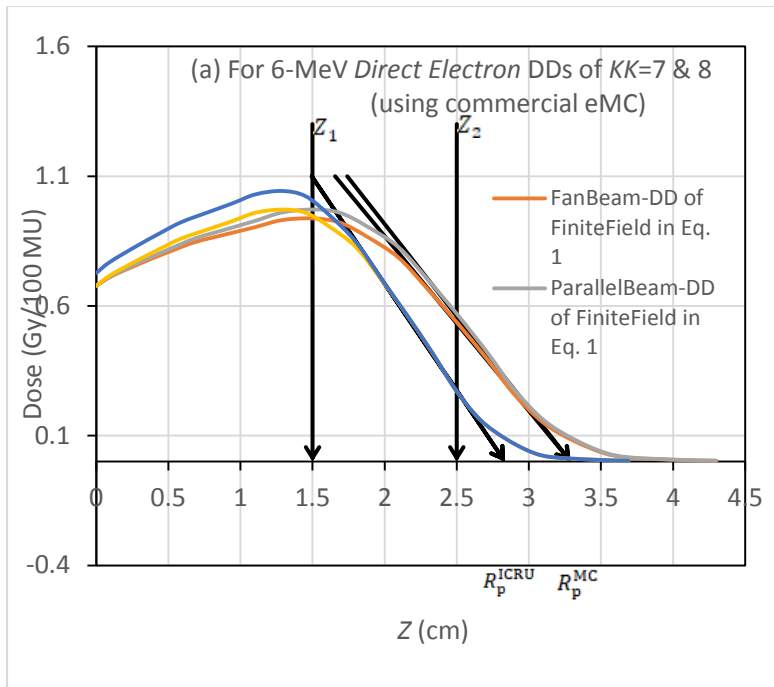


(b)

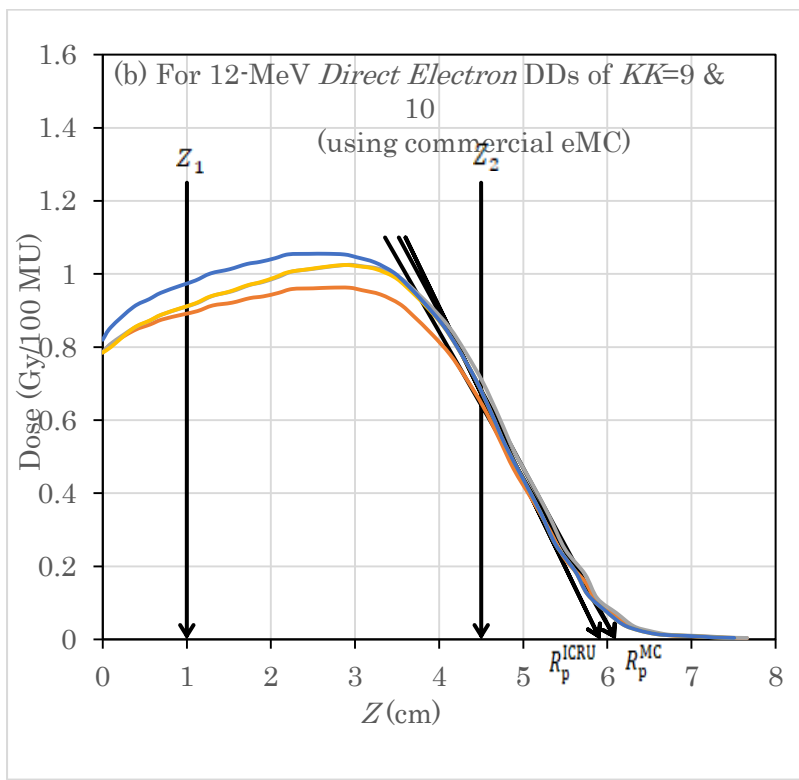


(c)

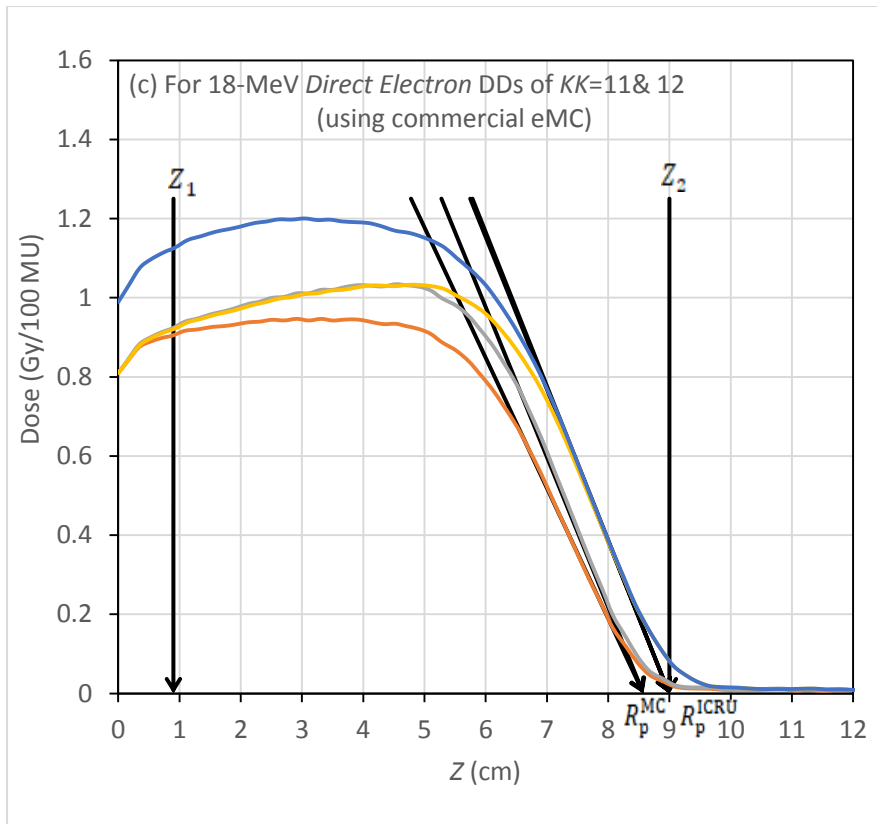
Supplementary Figure 9a-c Each of (a)-(c) diagrams showing a series of DD curves yielded using the standard eMC, reaching the corresponding parallel beam DD curve of infinite field ($A_0 = \infty$) used for direct electron beams, derived on the basis of the stepped DD-curves in (a) *Supp. fig. 1(a)* showing 6-MeV DD (KK=1 and 2), (b) *Supp. fig. 3(a)* showing 12-MeV DD (KK=3 and 4), and (c) *Supp. fig. 1(d)* showing 18-MeV DD (KK=5 and 6), as listed in Supplementary Table 1. In each DD group of (a)-(c), the first DD shows $D_{\text{fan}}(0,0,Z = Z':A_0)$ in Eq. 1 (orange line), the second DD shows $D'_{\text{para}}(0,0,Z = Z':A_0)$ in Eq. 1 (gray line), the third DD shows $D'_{\text{para}}(0,0,Z:A_0 = \infty)$ in Eq. 2 (yellow line), and the last DD shows $D_{\text{para}}(0,0,Z = Z_c^{\text{fan}}:A_0 = \infty)$ of Eq. 4 (blue line).



(a)

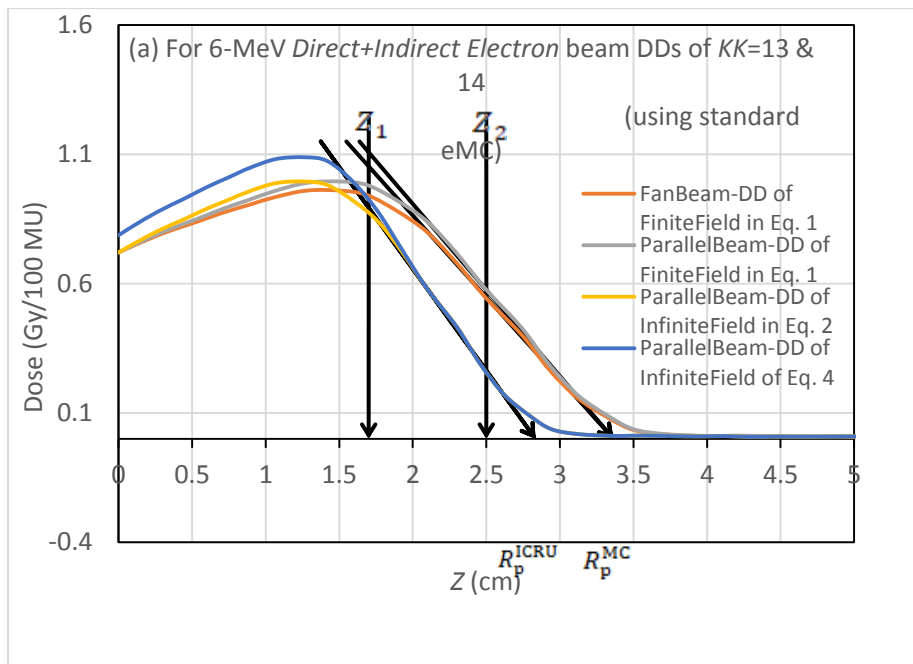


(b)

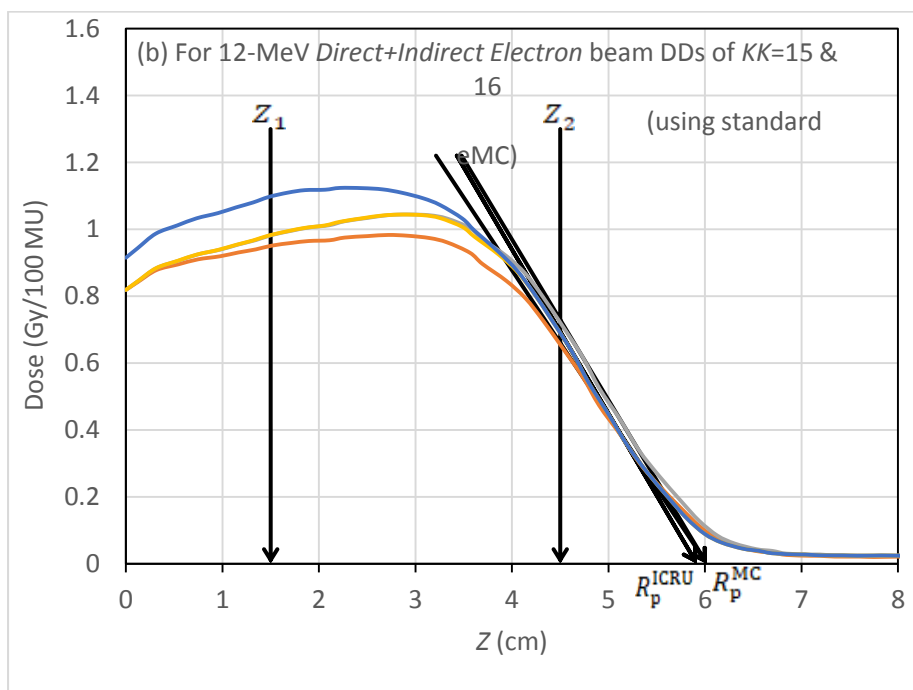


(c)

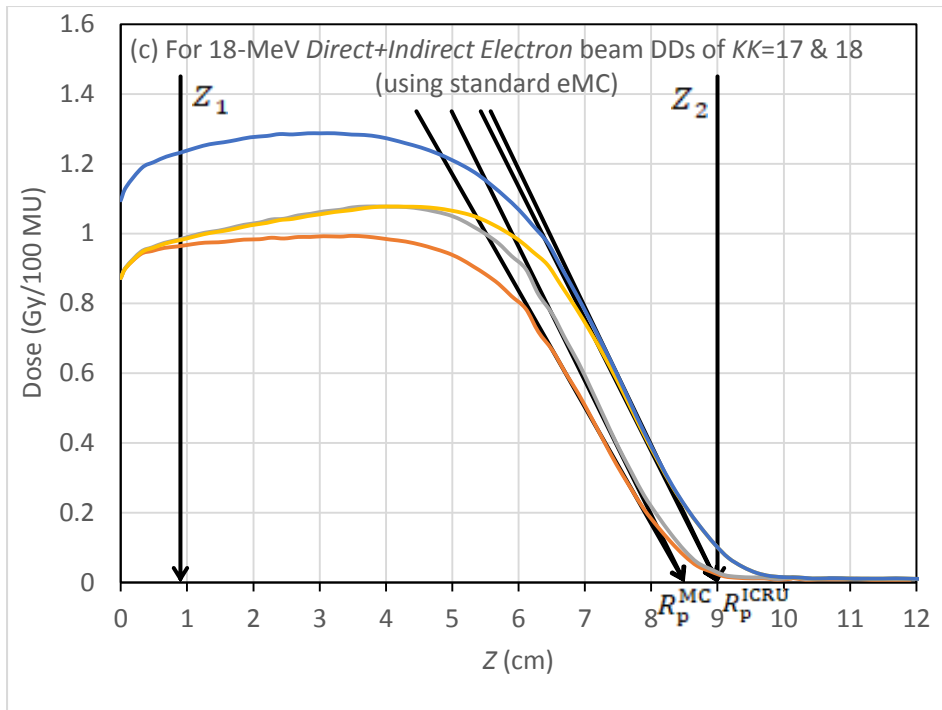
Supplementary Figure 10a-c Each of (a)-(c) diagrams showing a series of DD curves yielded using the commercial eMC, reaching the corresponding parallel beam DD curve of infinite field ($A_0 = \infty$) used for direct electron beams, derived on the basis of the dotted DD-curves in (a) *Supp. fig. 1(a)* showing 6-MeV DD (KK=7 and 8), (b) *Supp. fig. 3(a)* showing 12-MeV DD (KK=9 and 10), and (c) *Supp. fig. 1(d)* showing 18-MeV DD (KK=11 and 12), as listed in Supplementary Table 1. Further details are the same as in Supp. Fig. 9.



(a)

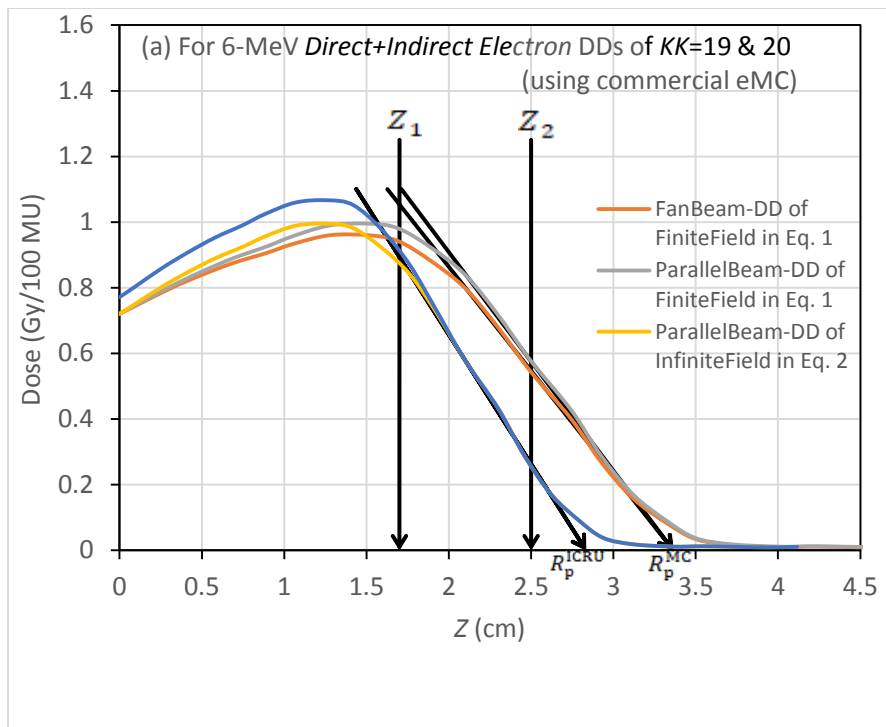


(b)

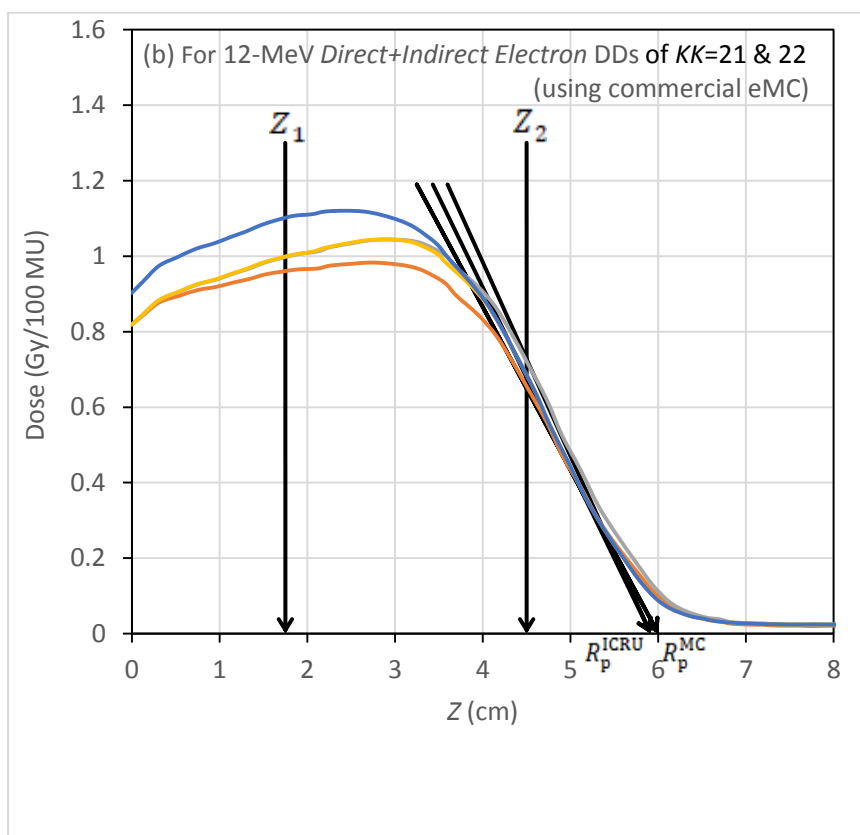


(c)

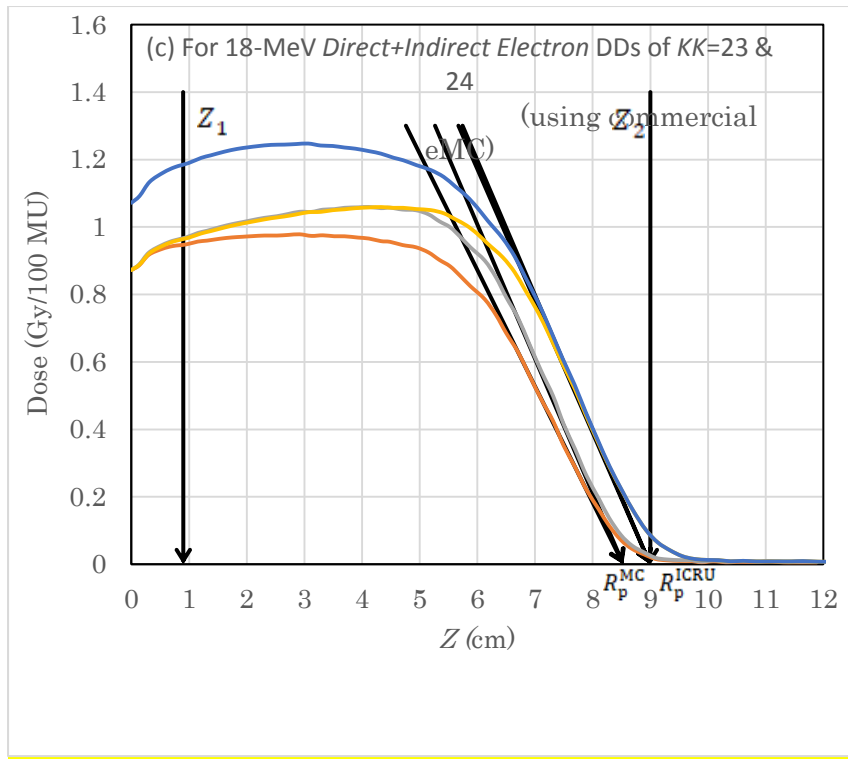
Supplementary Figure 11a-c Each of (a)-(c) diagrams showing a series of DD curves yielded using the standard eMC, reaching the corresponding parallel beam DD curve of infinite field ($A_0 = \infty$) used for direct-plus-indirect electron beams, derived on the basis of the stepped DD-curves in (a) *Supp. fig. 1(a)* showing 6-MeV DD (KK=13 and 14), (b) *Supp. fig. 3(a)* showing 12-MeV DD (KK=15 and 16), and (c) *Supp. fig. 1(d)* showing 18-MeV DD (KK=17 and 18), as listed in Supplementary Table 1. Further details are the same as in Supp. Fig. 9.



(a)

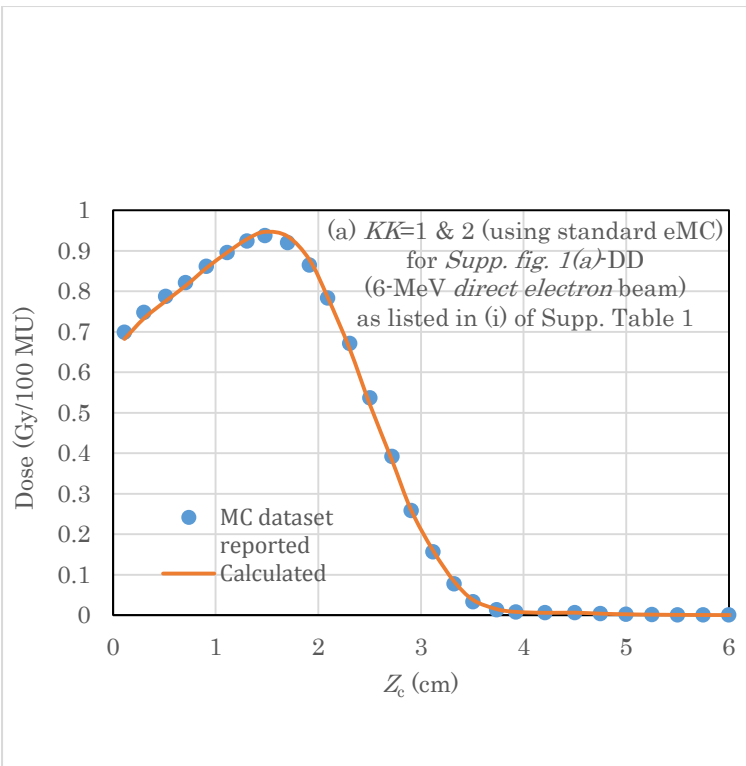


(b)

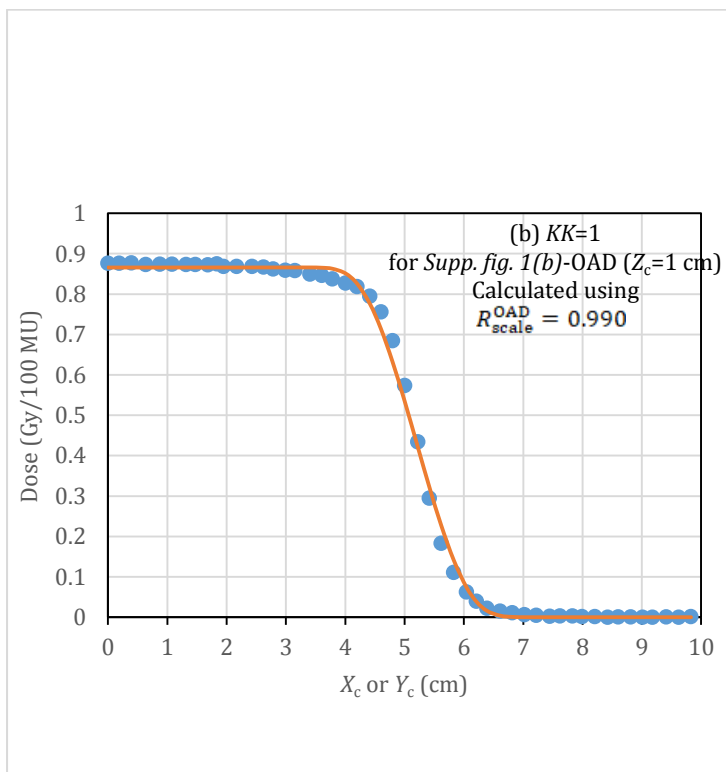


(c)

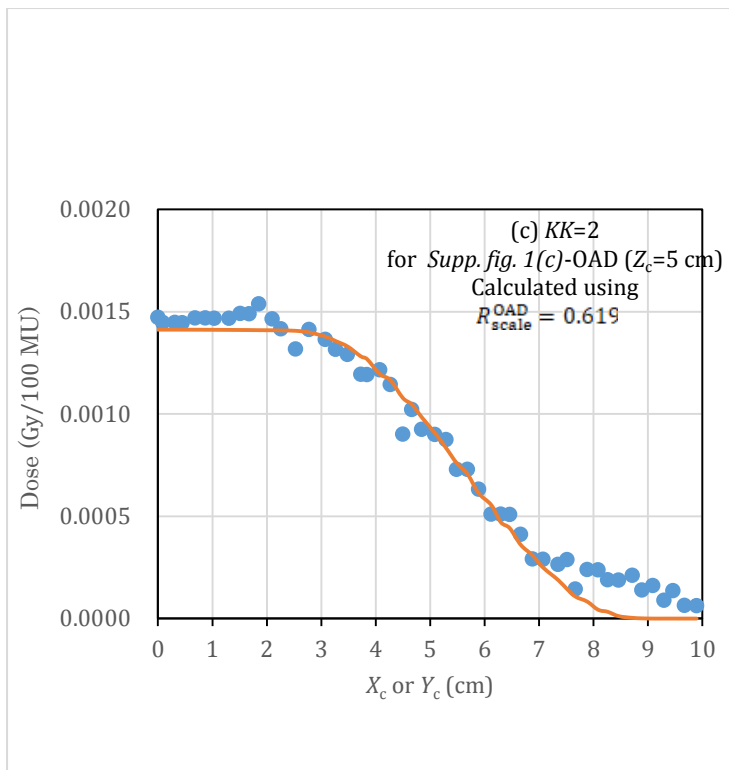
Supplementary Figure 12a-c Each of (a)-(c) diagrams showing a series of DD curves yielded using the commercial eMC, reaching the corresponding parallel beam DD curve of infinite field ($A_0 = \infty$) used for direct-plus-indirect electron beams, derived on the basis of the stepped DD-curves in (a) *Supp. fig. 1(a)* showing 6-MeV DD ($KK=19$ and 20), (b) *Supp. fig. 3(a)* showing 12-MeV DD ($KK=21$ and 22), and (c) *Supp. fig. 1(d)* showing 18-MeV DD ($KK=23$ and 24), as listed in Supplementary Table 1. Further details are the same as in Supp. Fig. 9.



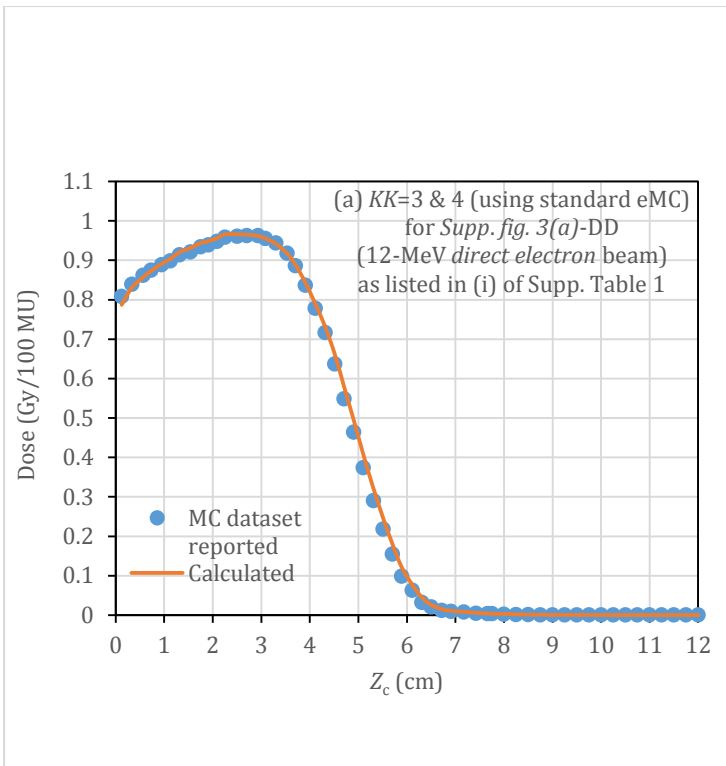
(a)



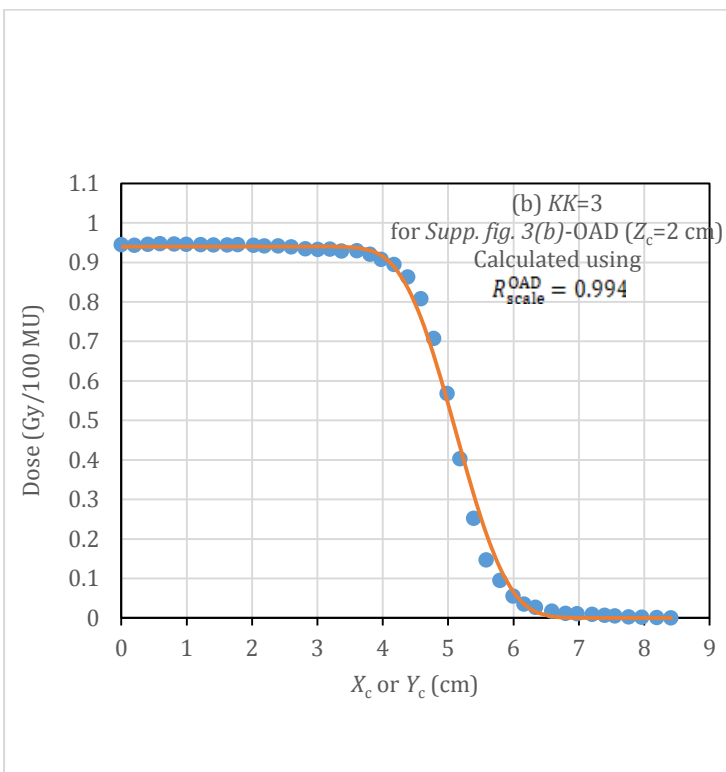
(b)



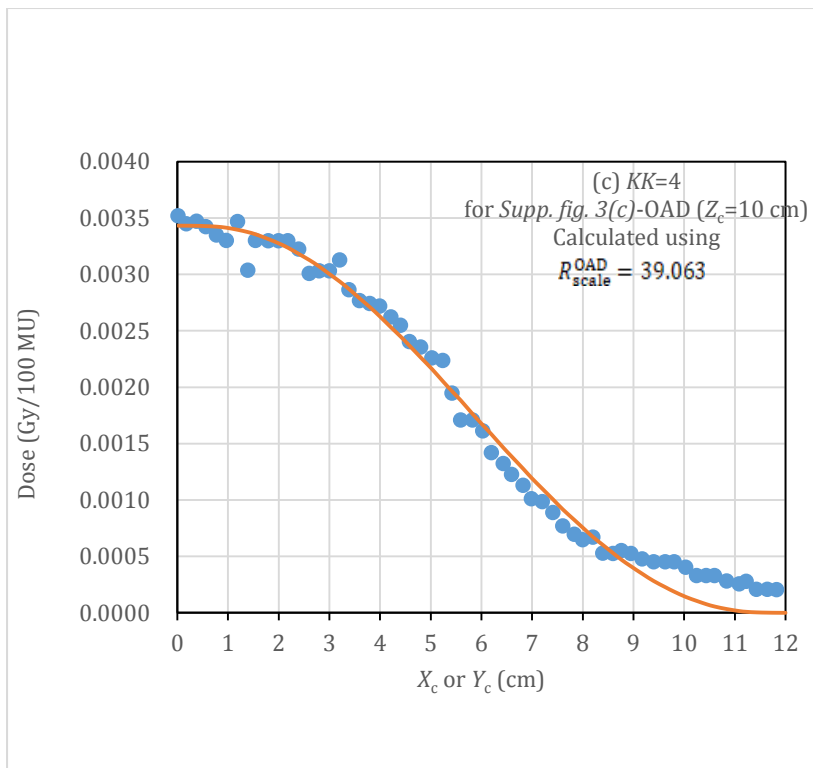
Supplementary Figure 13a-c One DD dataset in (a) and two OAD datasets on planes of (b) $Z_c = 1$ cm and (c) $Z_c = 5$ cm are illustrated for the 6-MeV *direct electron* beam, indicating $KK=1$ and 2 listed in (i) of Supplementary Table 1. Dots show the dose results with the standard eMC; and lines, the calculated dose results.



(a)

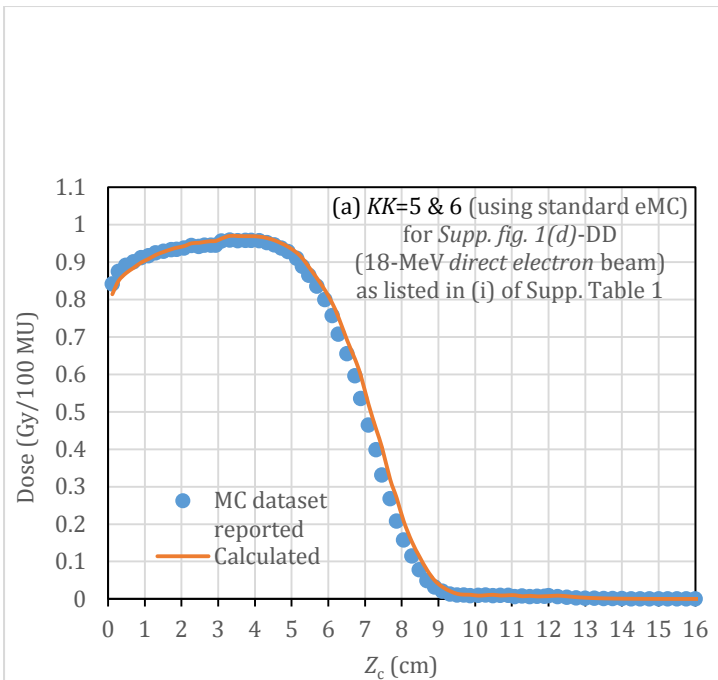


(b)

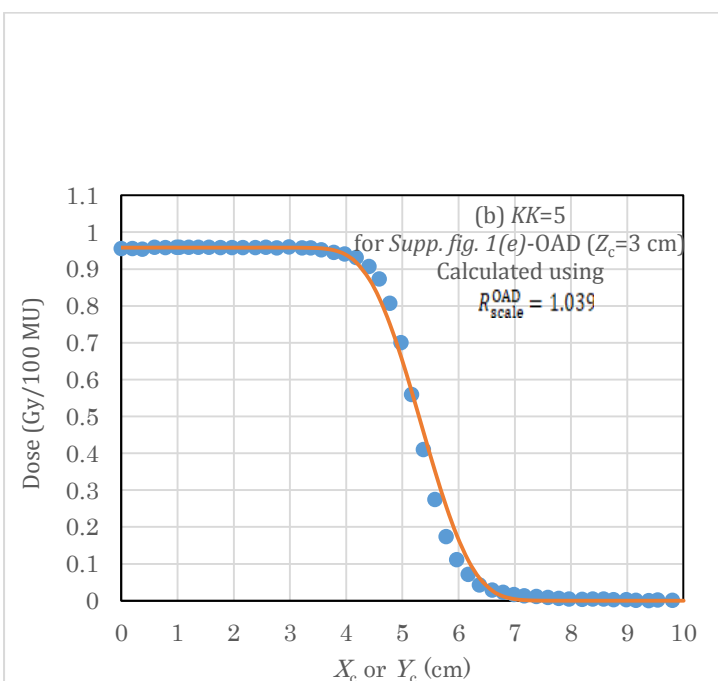


(c)

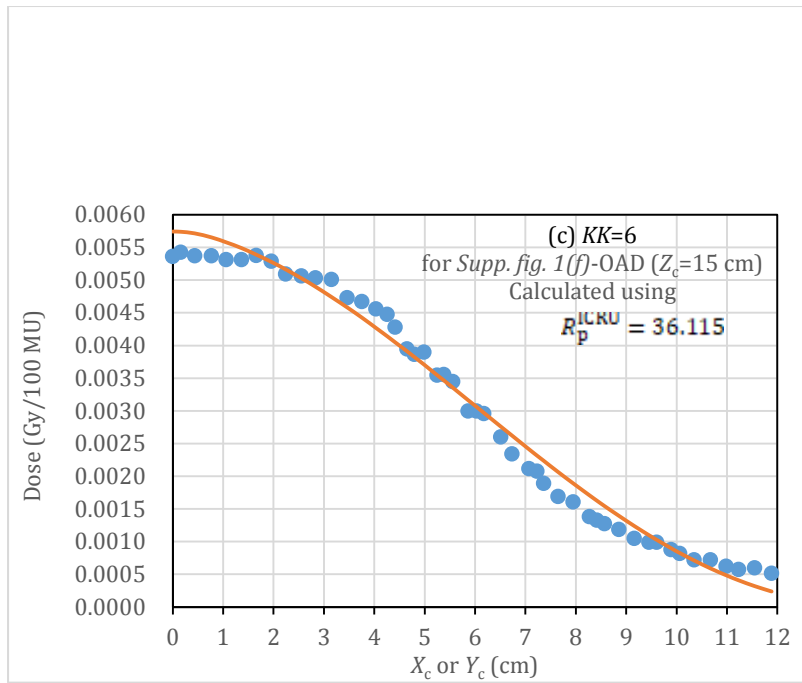
Supplementary Figure 14a-c One DD dataset in (a) and two OAD datasets on planes of (b) $Z_c = 2$ cm and (c) $Z_c = 10$ cm are illustrated for the 12-MeV *direct electron* beam, indicating $KK=3$ and 4 listed in (i) of Supplementary Table 1. Further details are the same as in Supp. Fig. 13.



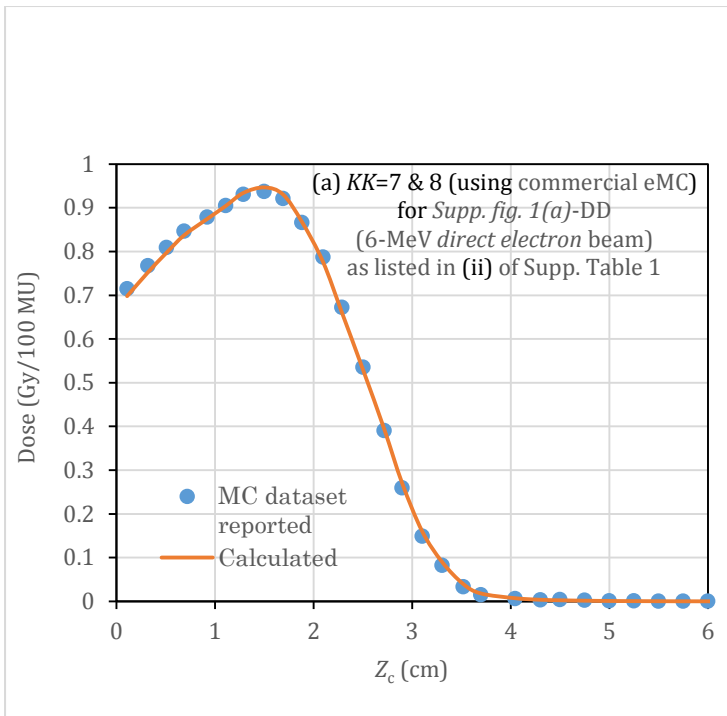
(a)



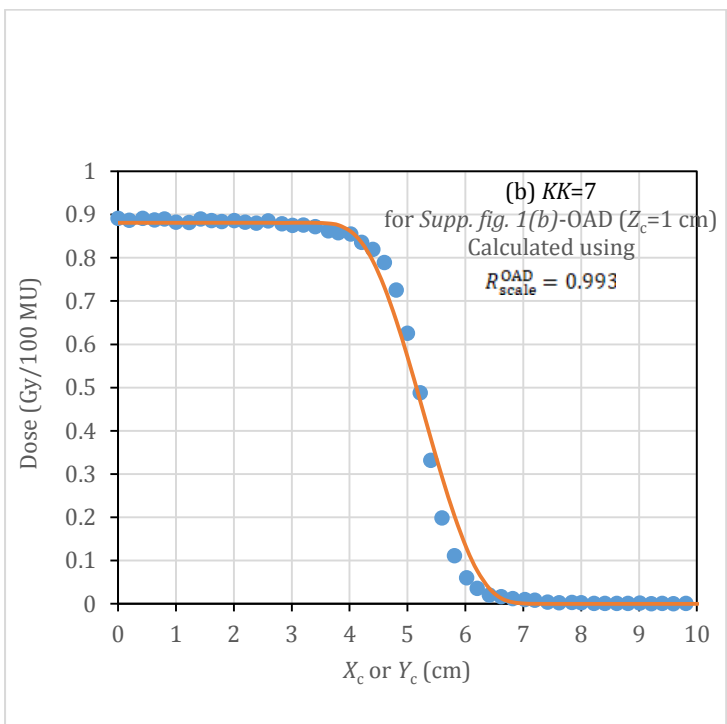
(b)



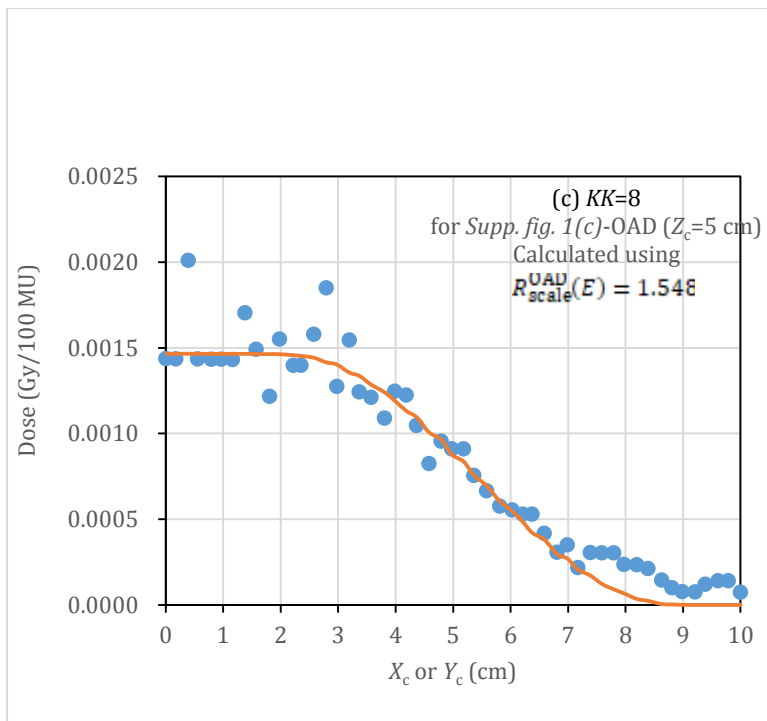
Supplementary Figure 15a-c One DD dataset in (a) and two OAD datasets on planes of (b) $Z_c = 3$ cm and (c) $Z_c = 15$ cm are illustrated for the 18-MeV *direct electron beam*, indicating $KK=5$ and 6 listed in (i) of Supplementary Table 1. Further details are the same as in Supp. Fig. 13.



(a)

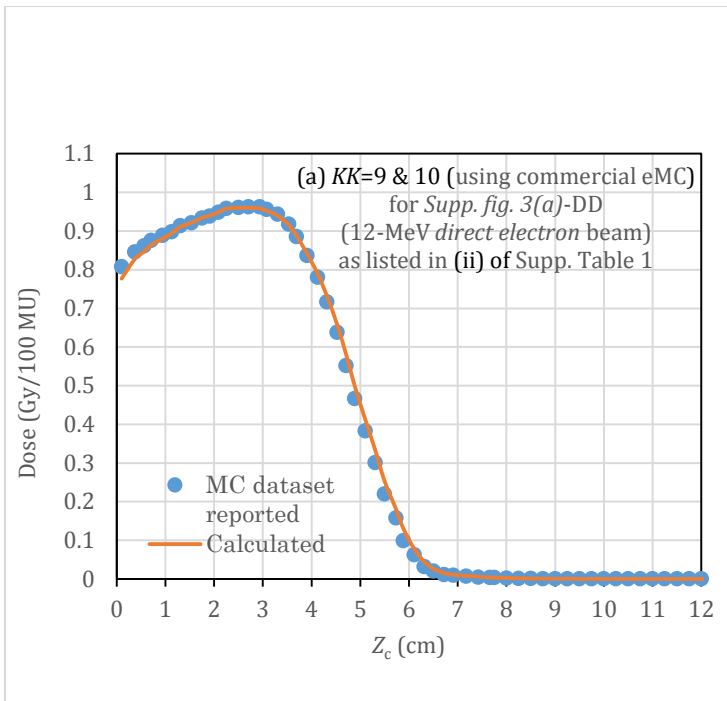


(b)

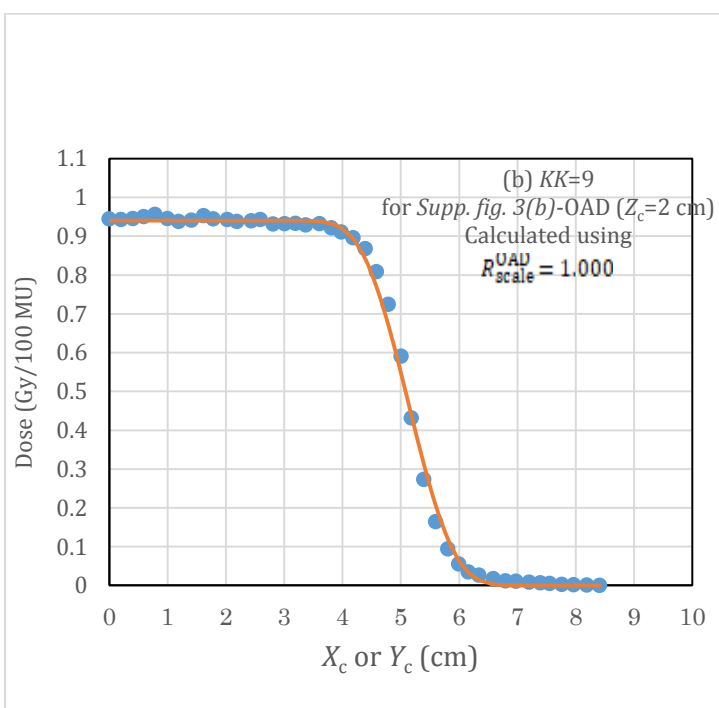


(c)

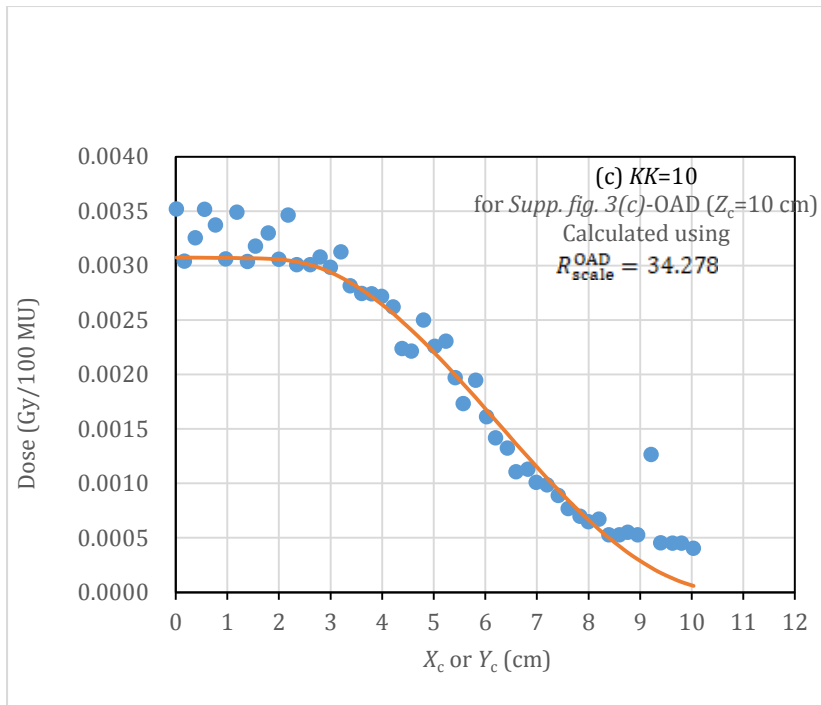
Supplementary Figure 16a-c One DD dataset in (a) and two OAD datasets on planes of (b) $Z_c = 1$ cm and (c) $Z_c = 5$ cm are illustrated for the 6-MeV *direct electron* beam, indicating $KK=7$ and 8 listed in (ii) of Supplementary Table 1. Dots show the dose results with the commercial eMC; and lines, the calculated dose results.



(a)

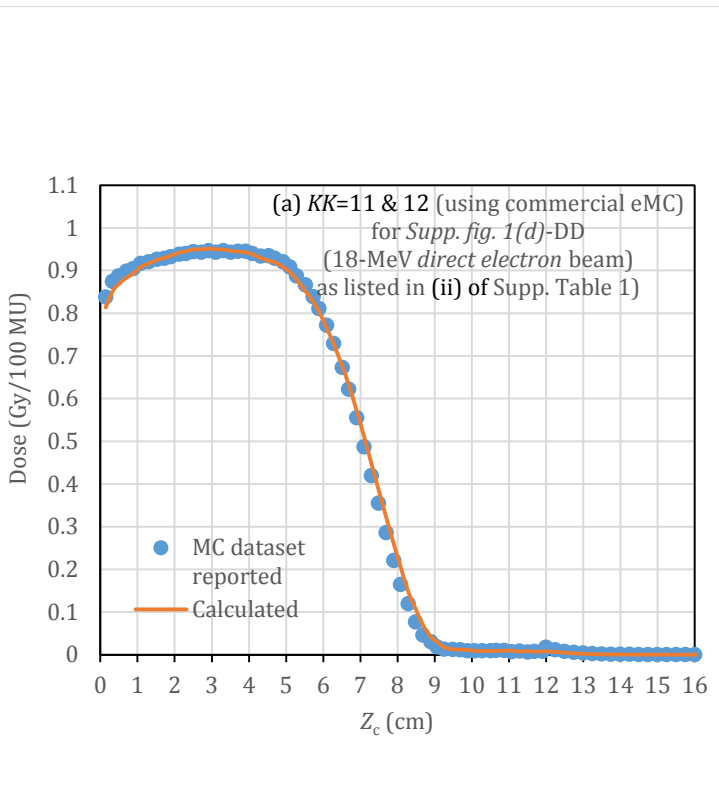


(b)

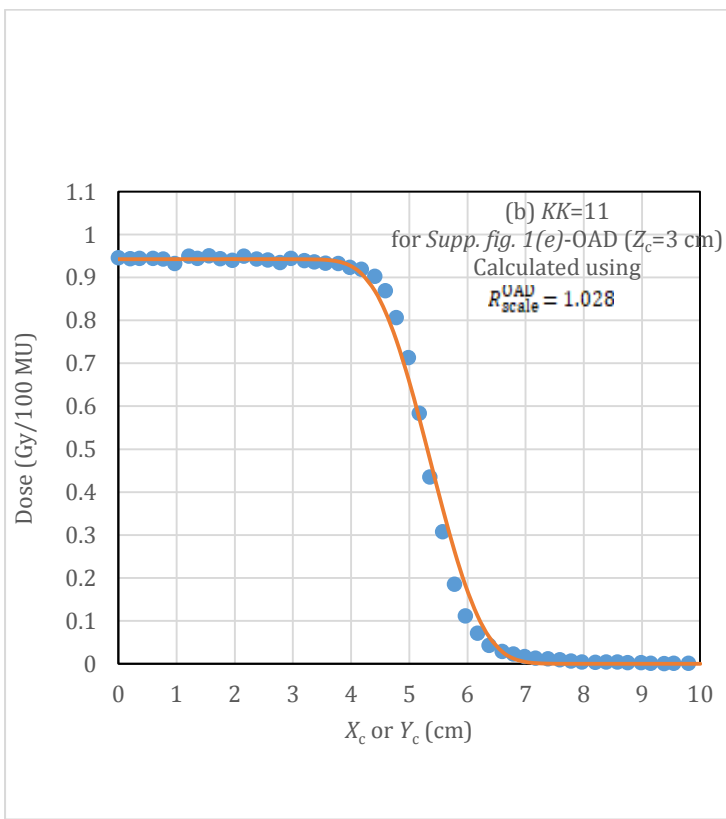


(c)

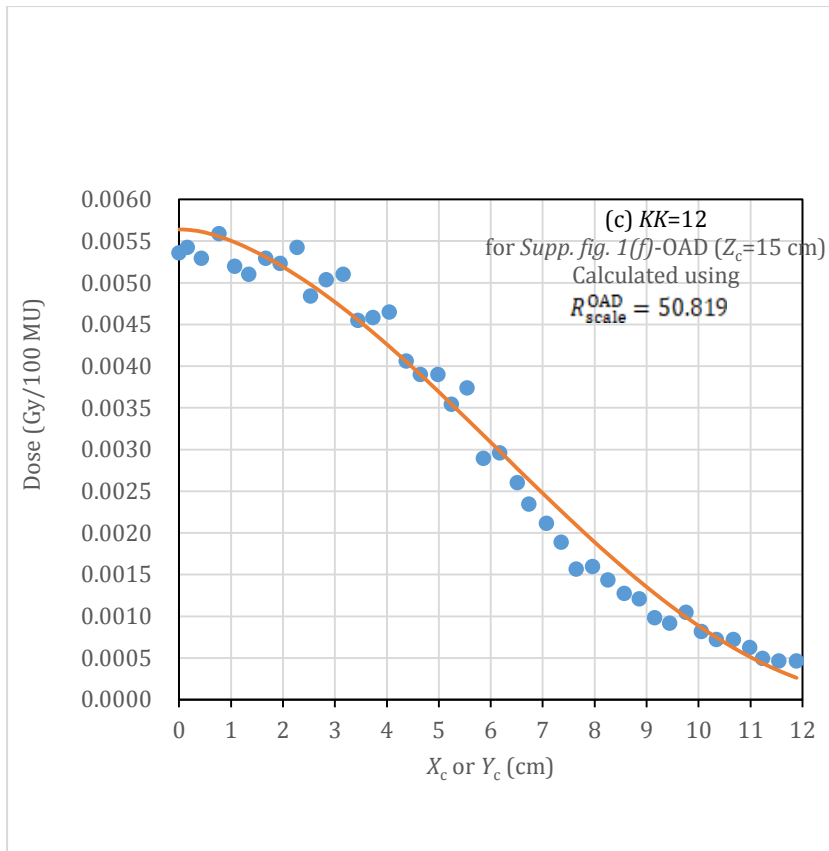
Supplementary Figure 17a-c One DD dataset in (a) and two OAD datasets on planes of (b) $Z_c = 2$ cm and (c) $Z_c = 10$ cm are illustrated for the 12-MeV *direct electron* beam, indicating KK=9 and 10 listed in (ii) of Supplementary Table 1. Further details are the same as in Supp. Fig. 16.



(a)

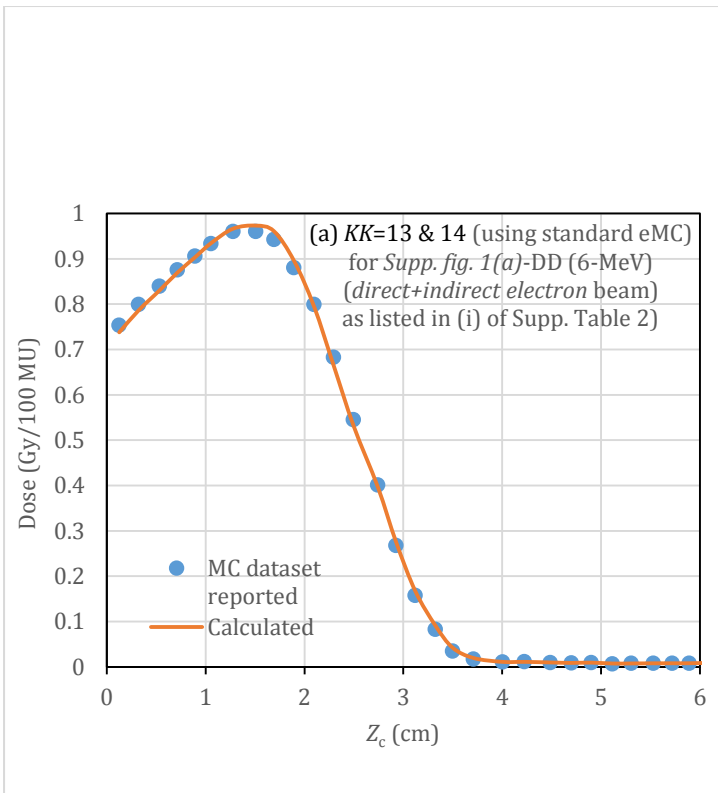


(b)

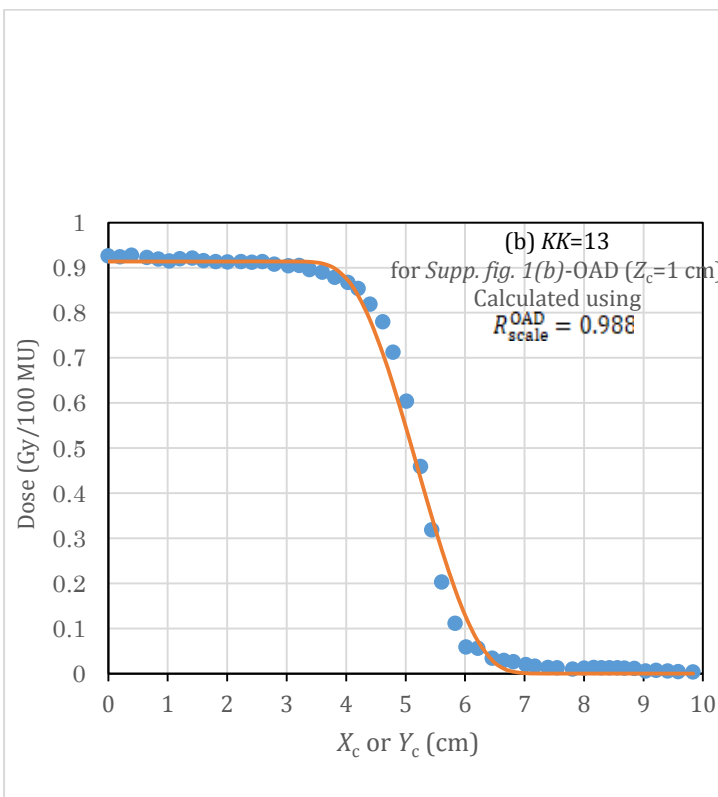


(c)

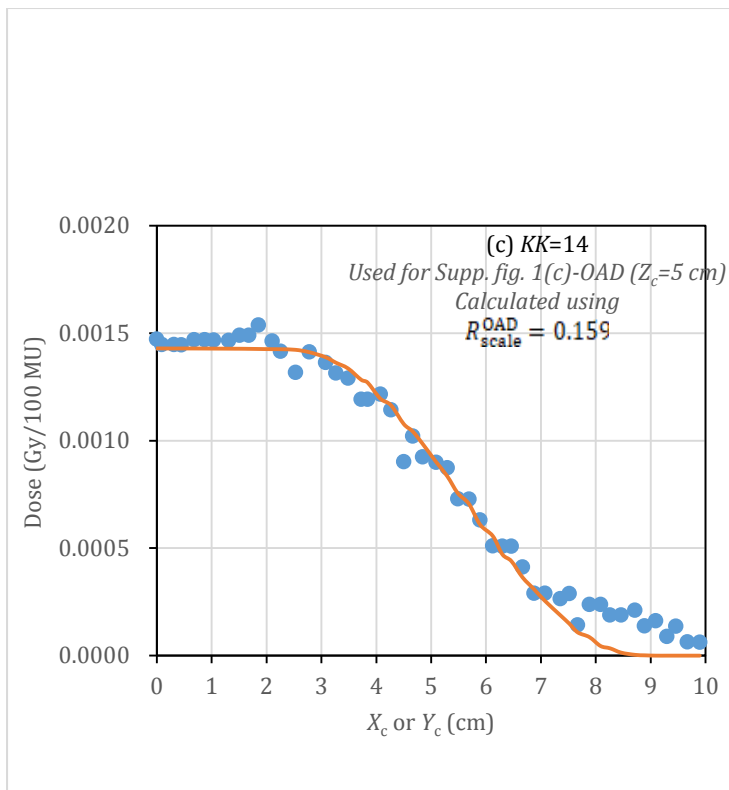
Supplementary Figure 18a-c One DD dataset in (a) and two OAD datasets on planes of (b) $Z_c = 3$ cm and (c) $Z_c = 15$ cm are illustrated for the 18-MeV *direct electron* beam, indicating $KK=11$ and 12 listed in (ii) of Supplementary Table 1. Further details are the same as in Supp. Fig. 16.



(a)

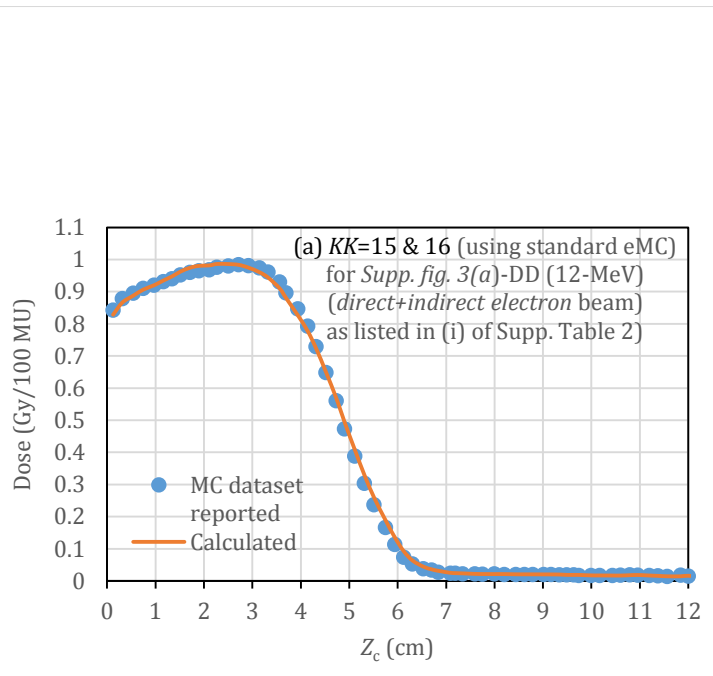


(b)

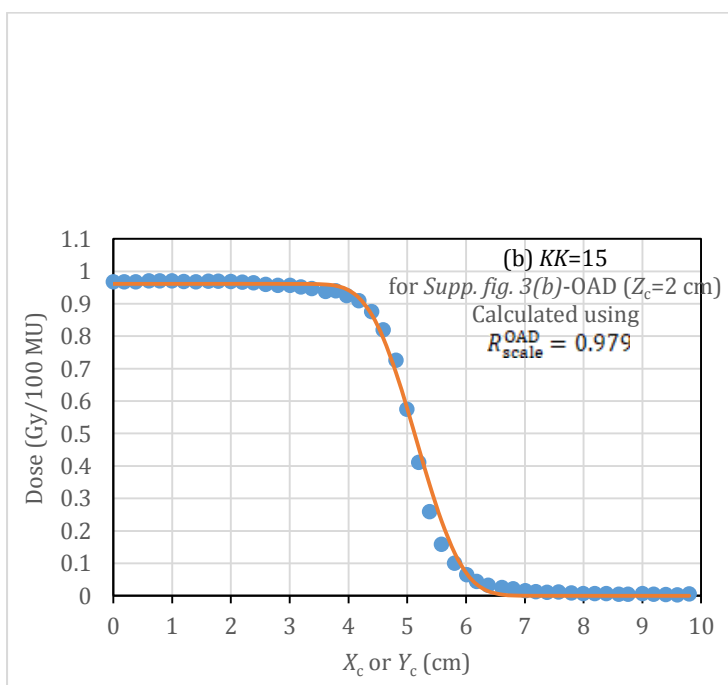


(c)

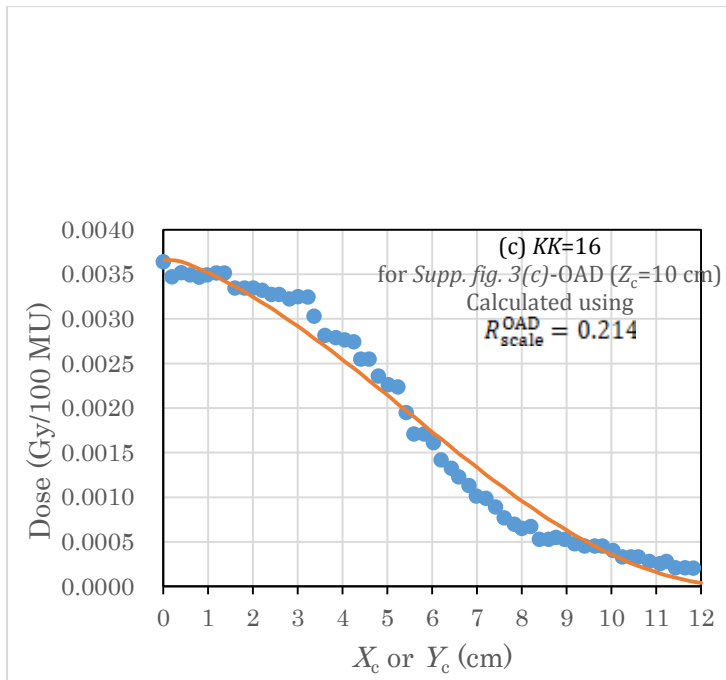
Supplementary Figure 19a-c One DD dataset in (a) and two OAD datasets on planes of (b) $Z_c = 1\text{ cm}$ and (c) $Z_c = 5\text{ cm}$ are illustrated for the 6-MeV *direct-plus-indirect electron beam*, indicating KK=13 and 14 listed in (i) of Supplementary Table 1. Dots show the dose results using the standard eMC; and lines, the calculated dose results.



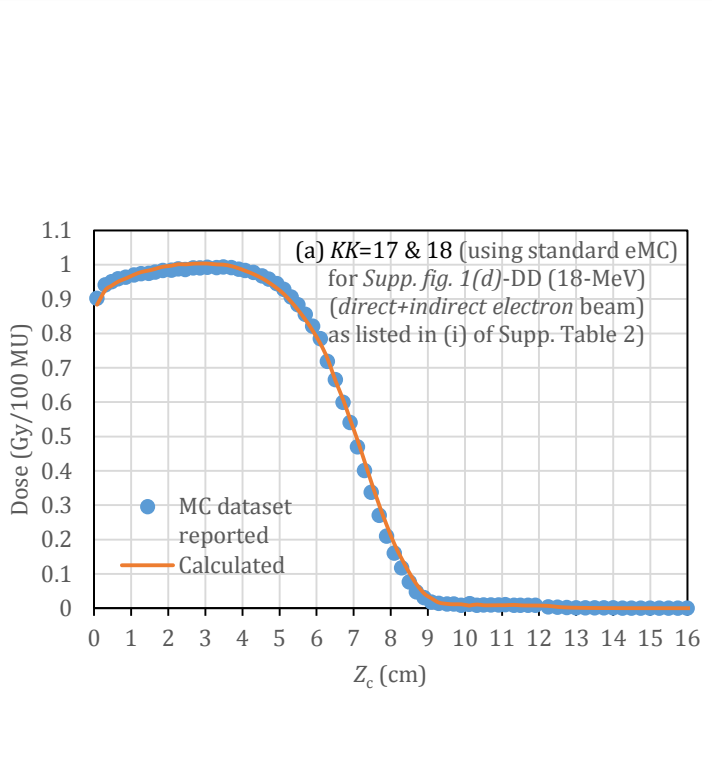
(a)



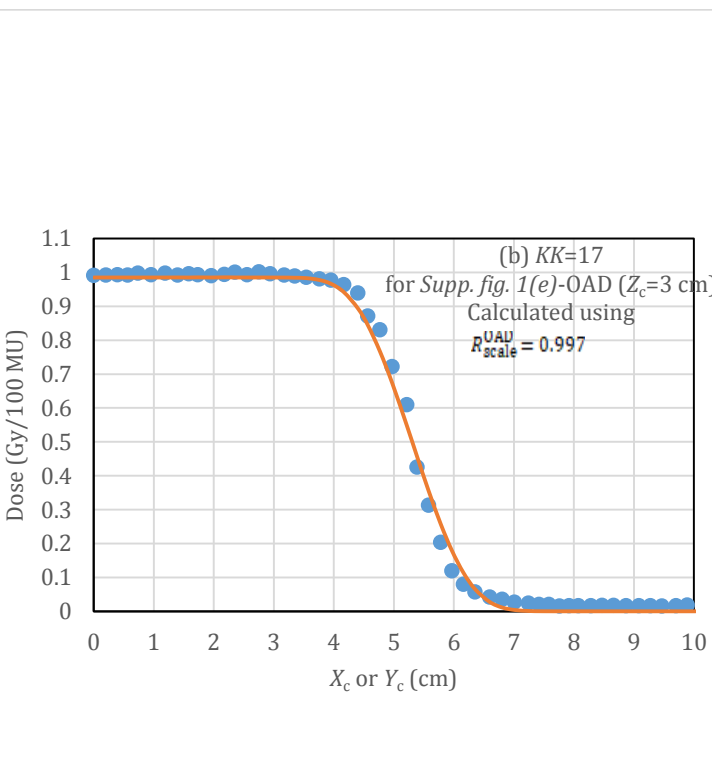
(b)



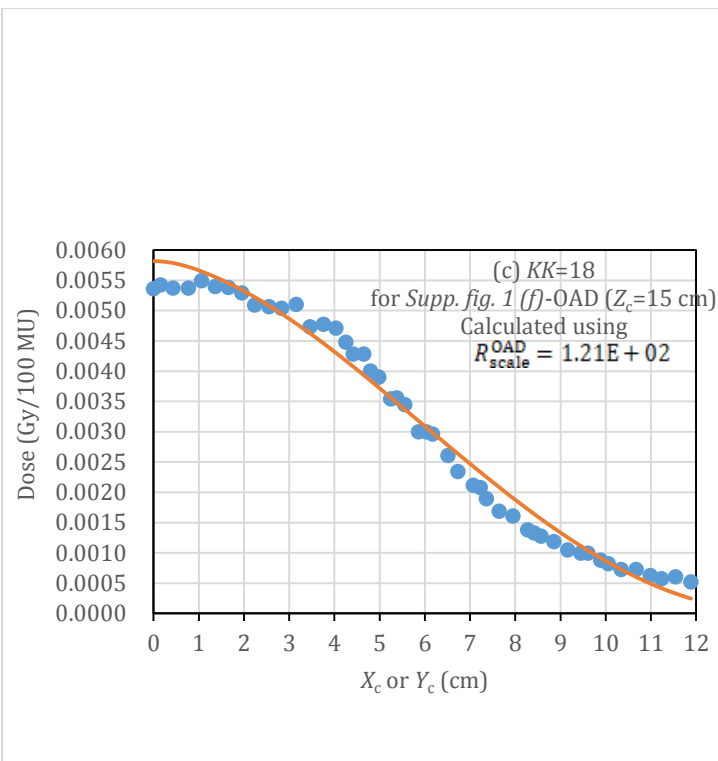
Supplementary Figure 20a-c One DD dataset in (a) and two OAD datasets on planes of (b) $Z_c = 2$ cm and (c) $Z_c = 10$ cm are illustrated for the 6-MeV *direct-plus-indirect electron* beam, indicating $KK=13$ and 14 listed in (i) of Supplementary Table 2. Further details are the same as in Supp. Fig. 19.



(a)

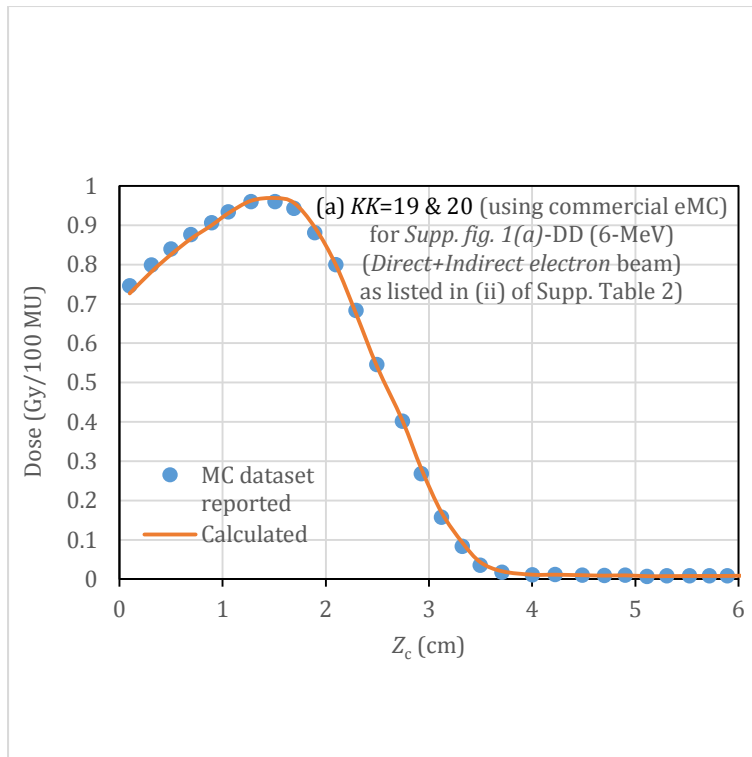


(b)

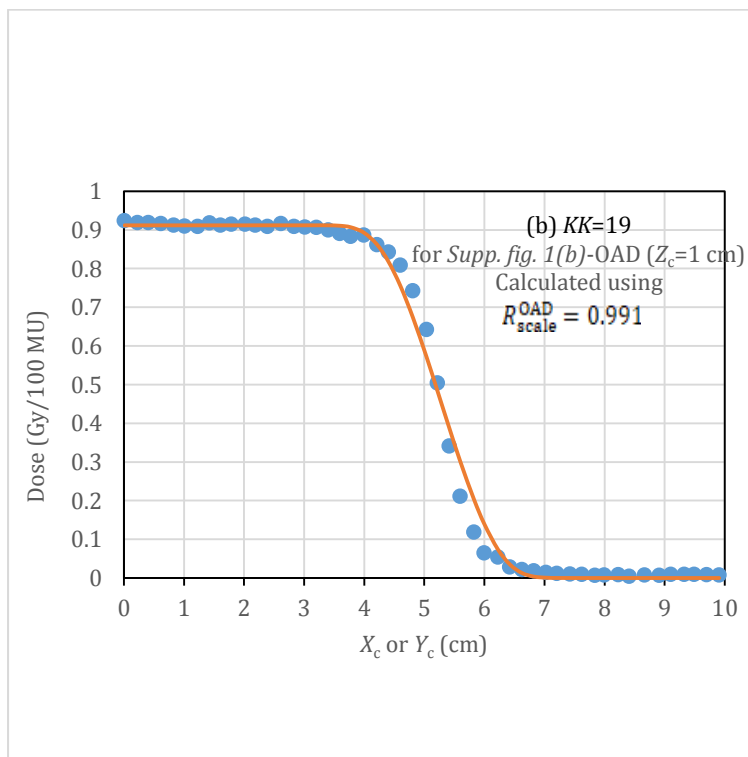


(c)

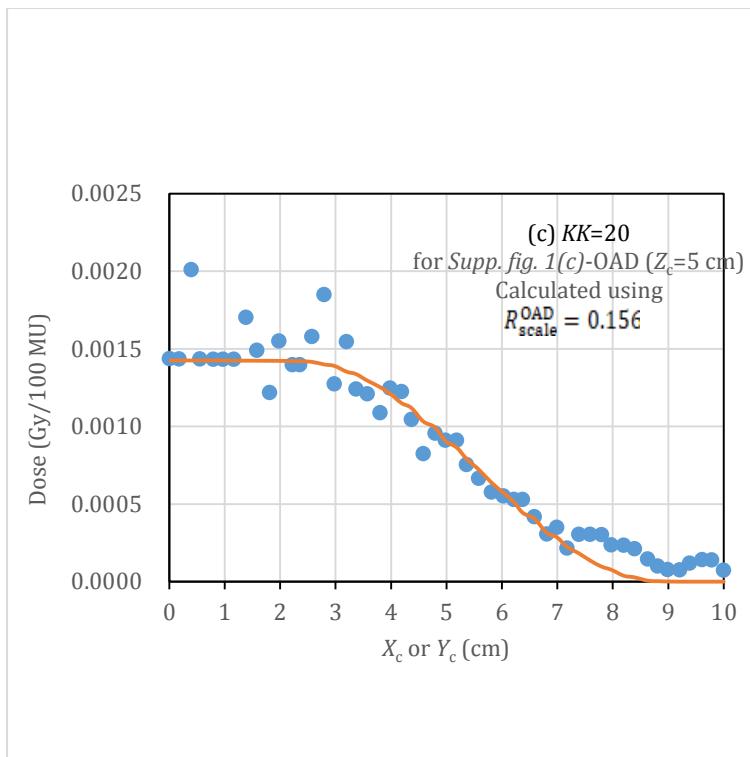
Supplementary Figure 21a-c One DD dataset in (a) and two OAD datasets on planes of (b) $Z_c = 3$ cm and (c) $Z_c = 15$ cm are illustrated for the 18-MeV *direct-plus-indirect electron beam*, indicating KK=17 and 18 listed in (i) of Supplementary Table 2. Further details are the same as in Supp. Fig. 19.



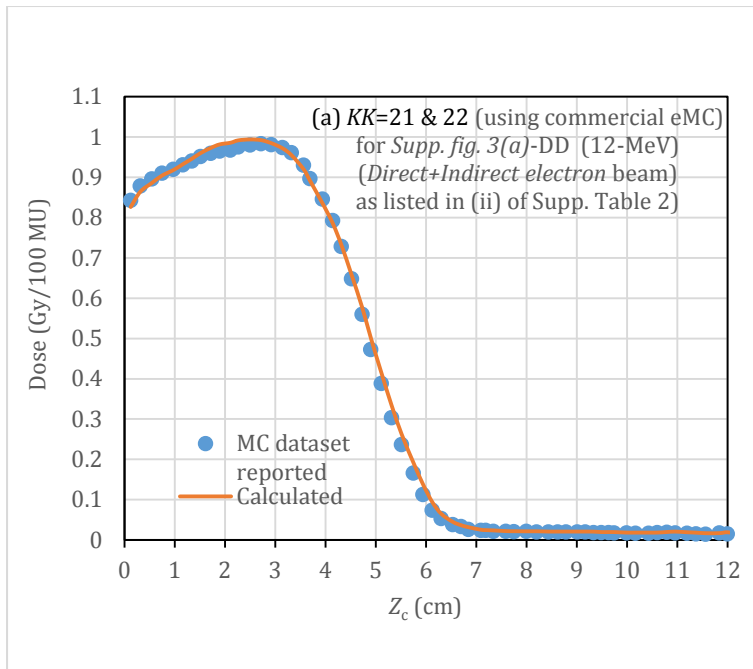
(a)



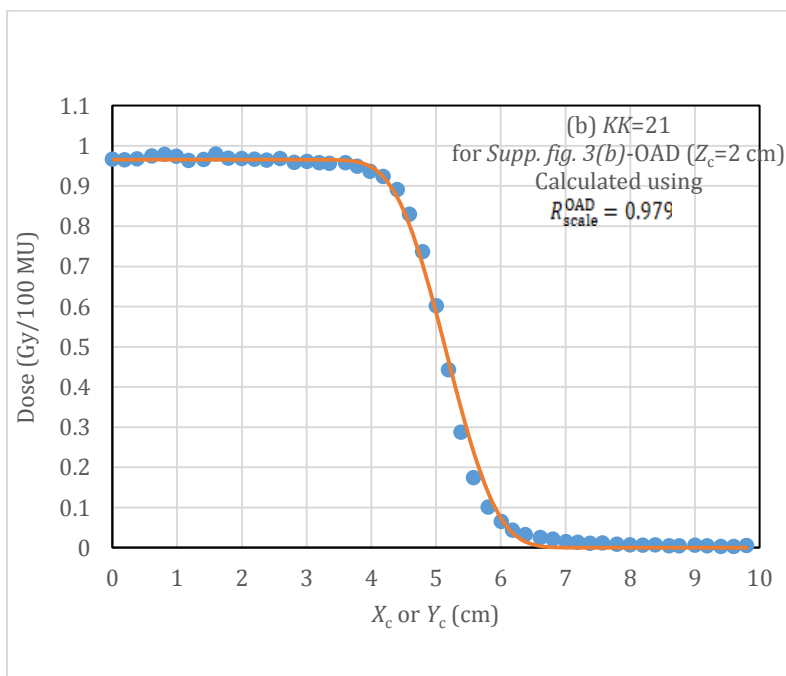
(b)



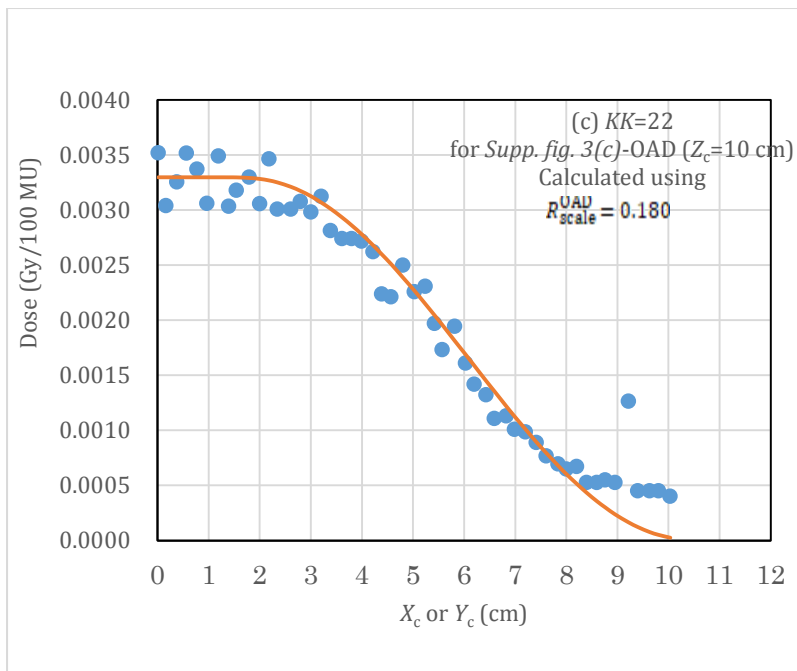
Supplementary Figure 22a-c One DD dataset in (a) and two OAD datasets on planes of (b) $Z_c = 1 \text{ cm}$ and (c) $Z_c = 5 \text{ cm}$ are illustrated for the 6-MeV *direct-plus-indirect electron* beam, indicating $KK=19$ and 20 listed in (ii) of Supplementary Table 2. Dots show the dose results of the commercial eMC; and lines, the calculated dose results.



(a)

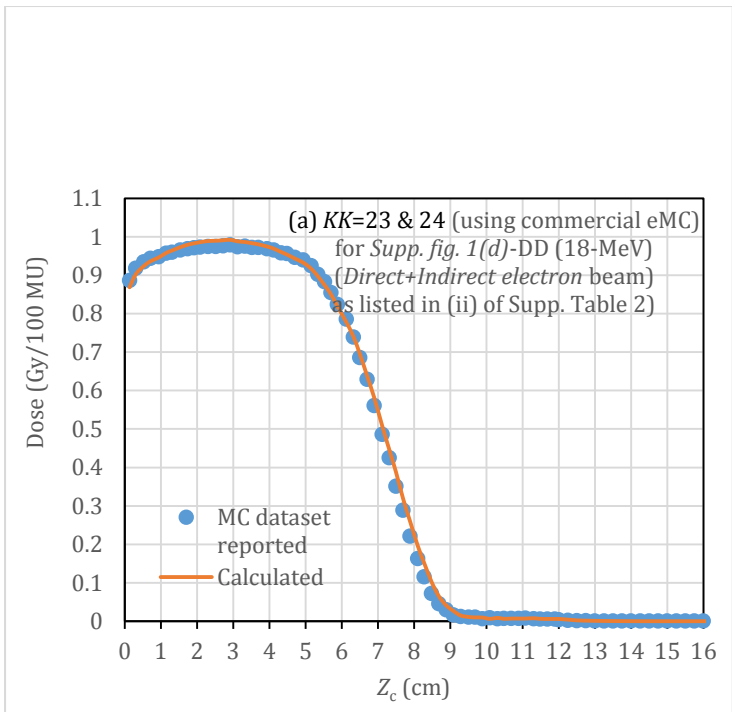


(b)

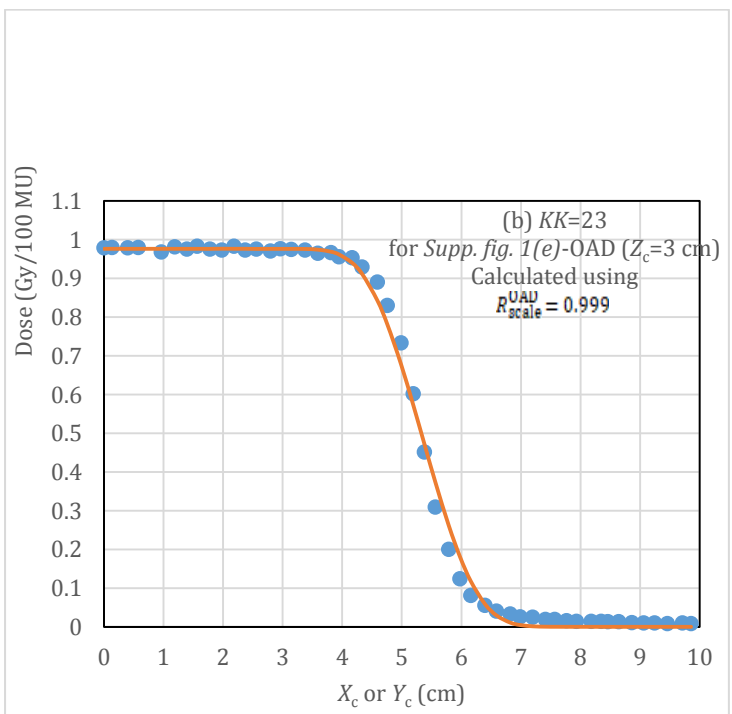


(c)

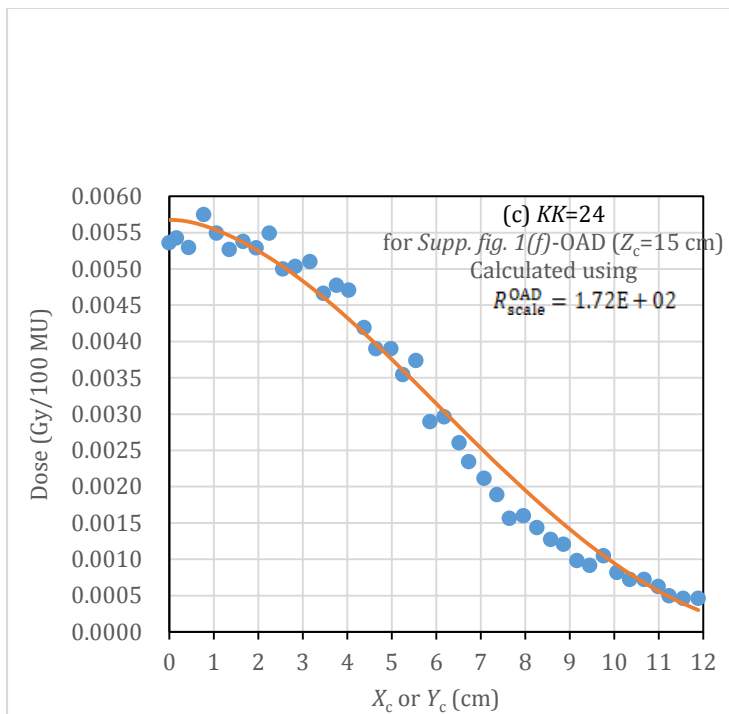
Supplementary Figure 23a-c One DD dataset in (a) and two OAD datasets on planes of (b) $Z_c = 2\text{ cm}$ and (c) $Z_c = 10\text{ cm}$ are illustrated for the 12-MeV *direct-plus-indirect electron beam*, indicating $KK=21$ and 22 listed in (ii) of Supplementary Table 2. Further details are the same as in Supp. Fig. 22.



(a)



(b)



(c)

Supplementary Figure 24a-c One DD dataset in (a) and two OAD datasets on planes of (b) $Z_c = 3$ cm and (c) $Z_c = 15$ cm are illustrated for the 18-MeV *direct-plus-indirect electron* beam, indicating $KK=23$ and 24 listed in (ii) of Supplementary Table 2. Further details are the same as in Supp. Fig. 22.